Accepted Manuscript

Model-Based Development Of A Fault Signature Matrix To Improve Solid Oxide Fuel Cell Systems On-Site Diagnosis

Pierpaolo Polverino, Cesare Pianese, Marco Sorrentino, Dario Marra

PII: S0378-7753(15)00038-5

DOI: 10.1016/j.jpowsour.2015.01.037

Reference: POWER 20473

To appear in: *Journal of Power Sources*

Received Date: 23 July 2014

Revised Date: 12 December 2014

Accepted Date: 6 January 2015

Please cite this article as: P. Polverino, C. Pianese, M. Sorrentino, D. Marra, Model-Based Development Of A Fault Signature Matrix To Improve Solid Oxide Fuel Cell Systems On-Site Diagnosis, *Journal of Power Sources* (2015), doi: 10.1016/j.jpowsour.2015.01.037.

HIGHLIGHTS

- An SOFC system dynamic model has been used to simulate normal and faulty conditions.
- An available Fault Signature Matrix based on Fault Tree Analysis has been improved.
- Missed fault and false alarm probabilities have been taken into account.
- Five faults have been simulated at stack and balance of plant level.
- Two threshold-dependent Modified Fault Signature Matrices have been obtained.

MODEL-BASED DEVELOPMENT OF A FAULT SIGNATURE MATRIX TO IMPROVE SOLID OXIDE FUEL CELL SYSTEMS ON-SITE DIAGNOSIS

Pierpaolo Polverino*, Cesare Pianese, Marco Sorrentino, Dario Marra

Department of Industrial Engineering, University of Salerno, Via Giovanni Paolo II 132 – 84084 Fisciano (SA)

*Corresponding author. Ph.: +39 089 96 4239; fax: +39 089 96 4037. E-mail address: ppolverino@unisa.it

ABSTRACT

The paper focuses on the design of a procedure for the development of an on-field diagnostic algorithm for solid oxide fuel cell (SOFC) systems. The diagnosis design phase relies on an in-deep analysis of the mutual interactions among all system components by exploiting the physical knowledge of the SOFC system as a whole. This phase consists of the Fault Tree Analysis (FTA), which identifies the correlations among possible faults and their corresponding symptoms at system components level. The main outcome of the FTA is an inferential isolation tool (Fault Signature Matrix - FSM), which univocally links the faults to the symptoms detected during the system monitoring. In this work the FTA is considered as a starting point to develop an improved FSM. Making use of a model-based investigation, a fault-to-symptoms dependency study is performed. To this purpose a dynamic model, previously developed by the authors, is exploited to simulate the system under faulty conditions. Five faults are simulated, one for the stack and four occurring at BOP level. Moreover, the robustness of the FSM design is increased by exploiting symptom thresholds defined for the investigation of the quantitative effects of the simulated faults on the affected variables.

Keywords: Solid Oxide Fuel Cell, Diagnosis, Model-based Modelling, Fault Simulation, Fault Signature Matrix.

1. INTRODUCTION

Nowadays the increasing interest on renewable energies drives the researchers activity towards new energy power systems, like Solid Oxide Fuel Cells (SOFCs). It is well known in literature that SOFCs are one of the most promising energy conversion systems due to several positive features: (i) high energy conversion efficiency, (ii) pollutants and green-house-gases emissions are limited as compared to other energy conversion systems, such as internal combustion engines, (iii) high flexibility and modularity, (iv) low acoustic emissions and (v) potential use in cogeneration applications, as a consequence of the high operating temperatures. Another important advantage is the possibility to exploit the internal reforming capabilities of SOFCs; therefore, simple pre-reformers can be implemented, thus allowing the more practical use of conventional fuels (e.g. Diesel, natural gas, methanol, propane, etc.), which in turn causes components manufacturing and system management costs reduction [1][2][3][4][5].

On the other hand, a wide commercial diffusion of these energy systems is hindered by materials and production costs and durability issues. It is well known that actual SOFC systems are characterized by low reliability of both stack and balance of plant (BOP), due to a large variety of possible degradation mechanisms and malfunctions that may occur in real world operation [1]. Indeed, degradation causes SOFC system lifetime not to be long enough with respect to durability requirements of either stationary (about 40,000 h with reference to e.g. residential or industrial Combined Heat and Power (CHP) systems [5]) or transportation (about 20,000 h with reference to e.g. Auxiliary Power Units – APUs [7]) applications [4][5]. In order to meet these lifetime targets, to improve degradation prevention capabilities and to optimize control actions, specific diagnosis methods are needed for real-time condition monitoring of the system. The development of an effective diagnostic algorithm, suitably coupled with adaptive control strategies, allows modifying the control laws while the system is running, thus resulting in both lifetime and performance improvement. Moreover, due to their intrinsic features, adaptive control algorithms require the development of dynamic models, with high prediction accuracy and fast computational time. The same characteristics are essential also for model-based diagnosis. This methodology entails developing a reliable and accurate model, which can simulate the monitored system in all operating conditions. Through the comparison between measured and simulated signals, a specific inference process leads to the estimation of the actual system status. Compared to traditional methods, like monitoring and automatic protection, the fault diagnosis supervision is the only one capable to detect incipient faults (early detection), with high accuracy both during steady and transient states and for several system components (process components, sensors, actuators, etc.) [8][9].

In the available literature, many publications deal with the development of physical models (i.e. lumped, 0-, 1-, 2- or even 3-D) of the SOFC stack and in some cases also the BOP. The use of a high order model (i.e. 2- or 3-D) usually guarantees high accuracy, but introduces undesired high computational burdens [1]. This latter feature is critical for on-

board application of models to be embedded into either control or diagnostic tools. Wang et al. [10] proposed a review of several modelling approaches for SOFCs, mainly related to diagnostic purposes. The authors offer a thorough analysis of the main advantages and drawbacks of the considered approach and focus on the purposes they are more suitable for. Barelli et al. [11] and Martinez et al. [12] studied hybrid systems based on the combination of an SOFC stack and a gas turbine. An interesting work has been carried out by Hajimolana et al. [13], who developed a dynamic modelling of a tubular SOFC supplied with ammonia instead of pure hydrogen. Other papers focuses on SOFC-based combined-heat and gas (CHP) systems [14][15]. Focusing on diagnosis, some authors have presented model-based diagnosis for SOFCs [1][16][5] and PEFCs [17][18][19], while the problem is widely faced for conventional energy systems like internal combustion engines [8][20][21], gas turbines [9] and other complex systems [22][23][24][25].

Furthermore, it is worth noticing that a certain number of models developed for diagnosis purposes are also based on equivalent circuit elements coupled with electrochemical impedance spectroscopy measurements, such as in [5][19][40][41] and [42], or on black-box modelling approaches, such as Neural Networks [43][44][45][46][47]. These argumentations well justify the need for a reliable and effective diagnostics able to quickly detect degradation behaviours and/or malfunction states in the whole system and to process an adaptive control strategy, to bring the system to optimal operation.

Generally, ensuring safe operation of a complex system entails suitably accounting for the direct and indirect interactions among the different devices together with their possible faulty states, in addition to the optimal operating set-points of the main variables and parameters. In this context, the availability of a reliable and accurate diagnostic algorithm enables checking and monitoring the system behaviour as well as inferring on its state of health, also allowing to perform on-board modification of system control laws. Focusing on diagnosis, it is well known that to prevent the failure of a generic system (e.g. mechanical and electric devices, energy conversion systems, etc.) the most obvious decision is to shut it down whenever an abnormal functioning is observed. Nevertheless, even if this action could seem the most logical one, in many cases it is not the most convenient or even feasible. In these cases, the remedial action must be taken while the system is in operation according to the specific time-constrains and the whole repairing costs [24]. Therefore, the capability to detect the occurrence of any faulty state and to identify its causes are critical tasks, which are strongly related to the design procedure of the diagnostic algorithm [4]. Indeed, the faulty states that can be detected in the system are only those included in the model and in the inference process [26].

Fault diagnosis activity typically involves three main processes [4][27] [28][17]: (i) fault detection, (ii) fault isolation and (iii) fault identification. The aim of the first process is to detect an undesired or faulty state of the monitored system. Then, the location of the fault can be determined into the system through the isolation process, identifying which is the

component (or the components) that is under undesired operating condition. Finally, the identification process leads to the evaluation of the fault size and its time-varying behaviour.

The design of a reliable diagnostic algorithm requires the physical knowledge of the whole SOFC system and an in-deep analysis of the mutual interactions among all system components. To achieve an effective diagnosis the design process has to be performed carefully and a key role is played by the identification of the correlations among possible faults or failures[1] and their corresponding symptoms at system components level. This identification is performed through the so-called Fault Tree Analysis (FTA) methodology, which is the starting point of the above mentioned design phase. The main outcome of the FTA is an inferential isolation tool (Fault Signature Matrix - FSM), which univocally links the faults to the symptoms detected during the on-line monitoring of the SOFC system.

During the detection process, the information acquired through measurement devices is exploited to obtain significant indicators of the system state. The generation of these indicators strictly depends on which is the methodology used for the detection. In literature [27][28][39][40], several methodologies are proposed, namely model-based, signal-based and knowledge-based, but in this paper only the model-based approach is considered. This choice is mainly motivated by two distinctive features that characterize the methodology with respect to both knowledge- and signal-based approaches: i) the availability of a model allows reducing the need for extended experimental data-set [29] and ii) the greater generalizability of the methodology due to the expected higher physical content retained by the diagnostic tool. These two features make this approach appealing for diagnostic applications destined to SOFC systems, for whom experimental data are usually not easy to measure and whose system characteristics and configurations change from one manufacturer to another. On the other hand signal- and knowledge-based algorithms require a large amount of complex experiments to be conducted in faulty conditions to correlate either signals or derived information to the faulty states. In some cases experiments could not be performed due to the complexity or the lack of knowledge on the faults to be reproduced, such as electrochemical-induced degradation processes. In such cases, an experiment that simulates or induces the fault may be set up for, e.g., catalyst or electrochemical performance degradation in fuel cells [30] or in other devices [31]. Therefore, experiments feasibility, costs and time issues may limit the development of signal- and knowledge-based diagnosis algorithms.

The presented research originates from previous works on FTA [4] and model-based diagnosis methodology [16], remarking the direct and indirect dependences among the SOFC system components during several faulty operation states. The purpose of this study is to perform a deeper fault-to-symptoms dependency study through the exploitation of a dynamic

[1]According to the common nomenclature on fault diagnosis [27][28] the term fault denotes unacceptable deviation (malfunction) of at least one characteristic property from the standard conditions whereas a failure is a permanent event causing the interruption of a required function.

model, previously developed by the authors [1][2][3], thus enhancing the robustness of the FSM. These works were developed in the framework of the European Project GENIUS [48], whose results led to another outstanding paper authored by Sorce et al. [39], which deals with Fault Detection and Isolation (FDI) study for SOFC systems.

The paper is structured as follows. Initially, an overview on the model-based diagnosis methodology is performed, highlighting the core features and the critical points, followed by a synthetic description of the FTA, mainly focusing on the process the development of the FSM is based on. Then, a brief description of the generic SOFC system, used for the FSM development, is given, accounting for the main components and their interactions. Afterwards, a theoretical explanation of the proposed SOFC system dynamic model is presented together with the description of the modifications introduced to simulate faulty states. Then, several malfunction behaviours are simulated and the arising symptoms are compared to those defined into the FSM, thus allowing to fully demonstrate the limitation of adopting a purely heuristic approach to develop an isolation tool.

2. NOMENCLATURE

Acronyms

AC	Alternate Current
APU	Auxiliary Power Unit
BOP	Balance od Plant
CHP	Combined Heat and Power
CPR	Critical Pressure Ratio
DC	Direct Current
FT	Fault Tree
FTA	Fault Tree Analysis
FSM	Fault Signature Matrix
MFSM	Modified Fault Signature Matrix
OC	Operating Condition
PEFC	Polymer Electrolyte Fuel Cell
PI	Proportional Integral
SOFC	Solid Oxide Fuel Cell

Roman Symbols

A	geometrical cell area [m^2]
A_{HE}	pre-heater heat exchange area [m^2]
A_{REF}	reformer heat exchange area [m^2]
C	fluid heat capacity [$J\ K^{-1}$]
c_p	specific heat capacity at constant pressure [$J\ Kg^{-1}\ K^{-1}$]
D	diameter [m]
$\dot{E}$	energy flow [W]
f	friction coefficient [-]
F	Faraday constant [$A\ mol^{-1}$]
J	current density [$A\ cm^{-2}$]
K	solid heat capacity [$J\ K^{-1}$]
k	isentropic coefficient [-]
L	length [m]
$\dot{m}$	mass flow [$kg\ s^{-1}$]
M	molar mass [$Kg\ mol^{-1}$]
$\dot{n}$	molar flow [$mol\ s^{-1}$]
N	noise
n_{cells}	cells number [-]
p	pressure [Pa]
P	power [W]
Q	thermal loss [W]
r	residual
R	universal gas constant [$J\ mol^{-1}\ K^{-1}$]
s	analytical symptom
t	time [s]
T	temperature [K]
v	velocity [$m\ s^{-1}$]
V	voltage [V]

U	heat exchanger transfer coefficient [W m^{-2} K^{-1}]
U_f	fuel utilisation [-]
X	input variables
Y	measured system variables
$\hat{Y}$	simulated system variables

Greek Symbols

β	pressure ratio [-]
ε	fault magnitude [-]
η	efficiency [-]
λ	excess of air [-]
ξ	fault magnitude [-]
ρ	density [kg m^{-3}]
τ	threshold
χ	fault magnitude [-]

Subscripts and superscripts

air	air at cathode side
amb	ambient
c	cold fluid
CH_4	methane
CMP	compressor
EM	electric motor
F	faulty
h	hot fluid
H	hole
H_2O	water
HE	*air* pre-heater
in	inlet
is	isentropic
O_2	oxygen

out outlet

PB post burner

REF reformer

3. MODEL-BASED FAULT DIAGNOSIS

The main aspects concerning the model-based fault diagnosis reside on the development of a numerical model able to simulate the monitored system in its global behaviour. The term *global* highlights the capability of the model to take into account both direct and indirect correlations among the system components, which is an essential aspect to perform a correct diagnosis [32]. This model can be exploited as a reference for the evaluation of the system status, implementing it in conjunction with the real system. According to a general model-based approach, the model can be run in parallel to the monitored system [8][20]. Thus, the real-time application of these numerical models requires, on one hand, high accuracy and reliability and, on the other hand, fast computational time. As represented in Figure 1, the main variables monitored on the real system (Y), affected by noise (N), are compared to those simulated by the process model, in order to generate a specific feature, called herein *residual*. A residual is defined as the difference between the output signals (Y) measured in the system and those ($\hat{Y}$) generated by the model [4][8][9][17][20][27][28] :

$$r = Y - \hat{Y} \tag{1}$$

To distinguish between normal and faulty behaviour, the residual is compared to a reference tolerance range, characterized by a threshold levels τ. This comparison leads to the generation of an *analytical symptom*, which is representative of the system state: if the residual falls within the tolerance range, the symptom is 0, otherwise, when the residual overcomes the reference thresholds, it becomes 1, as shown below [20]:

$$s = \begin{cases} 0 & if \quad |r| \le \tau \\ 1 & if \quad |r| > \tau \end{cases} \tag{2}$$

When a symptom is active an undesired (faulty) state is occurring in the system. According to this definition, each monitored variable is simulated through the model and all drifts from normal behaviours are collected into a symptoms' vector *s*. After having populated the symptoms' vector, the detection process ends with the following status check: if the vector has all 0, the system is working in normal conditions, while, if one or more symptoms are 1, an undesired behaviour is occurring in the system. It is worth observing that other approaches concerning the detection process are available in the literature. As an example, in the paper of Sorce et al. [39], the detection is achieved by means of the residuals behaviour analysis during simulated faulty states, achieved through their own system model. The obtained residuals are gathered into several fault maps, which replace analytical symptoms and are then used for fault detection and isolation. Henceforth, the isolation of a specific fault is performed by analysing the graphical behaviours of measured residuals, obtained during real system monitoring, and comparing them to the developed fault maps.

In the present paper, to identify the location of the malfunction, the symptoms' vector is compared to reference information, describing the links between faults and symptoms. A direct approach would be to determine experimentally these correlations inducing undesired state in the system and collecting the related symptoms, thus obtaining an *explicit knowledge base* [8]. Nevertheless, an *a priori knowledge* can also be exploited to gain these correlations, avoiding carrying out complex experimental activities on the system. Indeed, in many cases the BOP components are widely known and an extensive literature explains their behaviours. Thus, a heuristic approach, such as the well-known Fault Tree Analysis, can set the causal relations among faults and symptoms, leading to the definition of a Fault Signature Matrix (FSM), as detailed in the following section.

4. FAULT TREE ANALYSIS

The Fault Tree Analysis (FTA) is an analytical deductive technique that can outline all the likely ways in which a malfunction or undesired behaviour can occur in the system. This methodology starts from a specific fault (which is the *top event*) and investigates, through a physical knowledge of the system and following a top-down approach, all the possible causes (which are the *basic events*, or *symptoms*), from which the considered fault can result [4]. It is worth noting that this methodology gives only a qualitative correlation between faults and symptoms; besides, it is not a model for all possible

faults or symptoms of the system, but it takes into account only those assessed by the analyst [32]. Therefore, the major drawback of the FTA is the inability to detect faults that are not considered into the analysis [23]. Overcoming the drawbacks of the FTA approach is out of the scope of the presented activity, since the focus is on the FSM. Indeed, the paper aims at demonstrating that, once the links between the system faults and the affected system variables (symptoms) are defined through the FTA and detailed into the FSM, the proposed methodology can improve these links following a quantitative analysis, not accounted for by the FTA. Through this analysis it is possible to highlight the sensitivity of each monitored variable to the considered faults.

The main result of the FTA is the fault tree (FT), which is a graphic representation of the connections among a top event and all the related symptoms. These connections are expressed through Boolean operators (i.e. *gates*), which allow or prevent the fault flow through the tree from one level to another. The higher level of the FT is the top event (i.e. the fault or malfunction under study), while the other levels are represented by intermediate events, which are other minor faults that occur due to previous causes. The bottom level is represented by the basic events (the symptoms), which may also correspond to specific faults that are not further developable [32].

The drawing of several fault trees for most of the undesired events, which can occur into a complex system, such as SOFC systems, is particularly significant for the identification of the variables that must be measured or estimated (e.g. when a specific measurement device is not available or the variable is not physically measurable). This methodology leads to a robust selection of the monitored parameters, gained through a balance among variable significance (the number and type of faults whom is related to) and measurement costs and capability.

Once all the fault trees for a specific system are gathered, the defined correlations between faults and symptoms can be merged into a matrix, the FSM. This matrix is a 2-D one, in whose rows are listed the possible faults considered into the study, while the columns list all the collected symptoms, each one referring to a specific monitored system variable. When a symptom is related to a fault, the corresponding element into the matrix is equal to 1, otherwise it is 0. It is worth noting that all the rows in the FSM must be different from each other, to allow the correct and univocal isolation of the faults within the system.

In the following the main aspects of an FTA applied to an SOFC system, presented by the authors in a previous paper [4], are detailed: first the system and its main components are briefly described; then, a fault tree for one specific fault is highlighted; finally, the FSM is presented, which is used as starting point for the development of an improved one.

4.1 Solid Oxide Fuel Cell (SOFC) system

An SOFC system is usually designed in such a way as to ensure normal stack operation to be reached through the proper configuration and the optimized control of the auxiliary components. Therefore, the behaviour of the entire system relies not only on the performance of the SOFC stack but also on that of the BOP, which is prone to malfunctions and failures due to the high number of mechanical and electronic components.

A schematic representation of a generic SOFC system is presented in Figure 2 [1][4]. At the air side, the blower supplies the stack with the required amount of air, whose set-point temperature is achieved into the pre-heater. At the fuel side, the methane (or other hydrogen-rich fuels) is processed by the pre-reformer, which requires a specific amount of water and heat for the reforming process; the first one is stored in a water tank and its release is guaranteed by a controlled pump, while the heat is recovered from the post-burner exhaust gases. These latter, once they come out from the pre-reformer, are also used to heat up the air into the pre-heater and the remaining heat can be used for co-generation applications. Finally, the temperature of the gases exiting the SOFC stack is increased into the post-burner, to maximize the heat transfer among these gases and the fresh ones both at anode and cathode side. Furthermore, the electric power provided by the SOFC stack also requires power conditioning devices to convert the current from DC to AC and to boost the voltage.

4.2 Fault Tree Analysis application and Fault Signature Matrix development

The application of the FTA to the aforementioned SOFC system requires a deep knowledge of the interactions among the main components (Stack and BOP) and their complexity suggests analysing the faults at the component level [4]. An example of FT for the air blower is proposed in Figure 3. As previously stated, the air blower feeds the stack with the required amount of air. Due to the high volume flow usually required, the compressor is the most energy consuming device of the system [4] and it is prone to several types of faults and malfunctions, some of them listed in Figure 3. It is clear that both the increase in compressor motor friction (e.g. bearings wear malfunctions) and the excessive overheating (e.g. lack of lubricant) are linked to the air outlet temperature and compressor power increase, whereas, if an air leakage in the inlet compressor manifold occurs, both the downstream pressure and the air pipe flow are affected.

Following the same approach for all the components, a set of FTs can be developed by taking into account the interactions among all the devices. From these FTs, a set of monitored variables can be drawn out, resolving a compromise among measurement costs, methodology robustness and reliability. Merging all the information obtained through the FTs, an FSM can be built, as shown in Table 1. According to this FSM, the faults taken into account in this work are:

- Fault f_1: air blower fault induced by an increase in its mechanical losses;
- Fault f_2: air leakage in the pipeline linking the air blower to the air pre-heater;
- Fault f_3: temperature controller failure;
- Fault f_4: pre-reformer fault produced by its heat exchange surface corrosion;
- Fault f_5: stack fault caused by an increase in its polarization losses;

From the FSM presented in [4] three modifications have been made. First of all, from the symptoms listed in that FSM, the current density has been removed. This choice is consistent with the assumption of taking the current density as a controlled input of the model; it is worth remarking that this variable is assumed as the ratio between the current load and the geometrical cell area, as detailed in section 6. Therefore, the number of symptoms is reduced from fifteen to fourteen. The second variation resides in the association of the pre-reformer fault (i.e. fault f_4 in Table 1) to an undesired event caused by heat exchange surface corrosion rather than catalyst degradation. According to the pre-reformer fault tree presented by Arsie et al. [4], the variables (i.e. the symptoms) affected by these faults are the same except for a possible increase in the pressure drop. However, since this last variable is not monitored (i.e. not considered in the FSM), the symptoms' vector proposed in [4] can be used as a reference for both the catalyst degradation and the heat exchange surface corrosion. The third modification consists in the association of the stack fault to an increase in the polarization losses, instead of a reduction in the surface active area, as considered instead by Arsie et al. [4]. According to the related fault tree, presented in [4], the only variation in the symptoms' vector is linked to the current density symptom, which turns from 1 to 0. However, since the current density is no more a symptom, the symptoms' vector proposed in [4] can be still used as a reference for the considered fault.

It is worth noting that to have a robust fault detection process the rows of the FSM should be as much independent each other as possible, which requires a large number of symptoms. However, observing the two last symptoms' vectors of the FSM of Table 1, they show the same pattern, hindering the univocal isolation of the two related faults. Nevertheless, as showed in the following paragraphs. this problem can be solved by performing a quantitative analysis on the relationships between faults and monitored variables.

5. THRESHOLD DESIGN

The selection of the proper threshold levels, which lead to the generation of symptoms through the comparison with the residuals (see Eq. (1) and Eq. (2)), is a very critical task; indeed, these values must take into account model inaccuracy and disturbances (i.e. signal noise). In case of low noise levels, a simple threshold value can be used, while, for high noise levels, a more advanced approach (e.g. statistics, fuzzy-logic, Kalman filters, etc.) should be implemented [9][23]. On the other hand, the right choice of thresholds values must fulfil the trade-off between robust diagnosis and early detection [20]. The knowledge of the devices installed on the real system, along with accuracy and resolution of the associated measured signals are key parameters to fix the thresholds. If poor resolution is available for the measures (Y in Eq. 1) due to, e.g., cheap instruments or low sensitivity, the residuals could always overcome the thresholds, resulting in a continuous faulty state. On the other hand, the thresholds must be set as lower as possible to be able to detect incipient faults.

An example of how a symptom arises is given in Figure 4: the comparison between the residual time behaviour r with the threshold level τ' leads to the symptom time behaviour S' (dotted line), in which two faulty states are detected; whereas if the residual is compared to the threshold τ'', the symptom time behaviour S'' (straight line) shows only one faulty state. Focusing on Figure 4, it is important to highlight that the first faulty state of the symptom time behaviour S' might not be a real faulty state but a false alarm. For this reason, another crucial aspect of the threshold selection is the capability to distinguish between false alarm and missed faults. The upper part of Figure 5 sketches the deterministic process followed for the symptoms generation process shown in Figure 4.

Considering stochastic behaviours of the residuals, the probabilities of missing a fault or incurring into a false alarm can be set for each symptom. This can be achieved when the probabilistic distribution of the monitored variables both in normal and faulty state are available from dedicated experimental activities. Then, the threshold could be set according to different probabilities of missed fault or false alarm, as shown in the lower part of Figure 5. It is possible to correlate to each threshold level the probabilities of false alarm and misdetection, which can be obtained through the intersection between the threshold value and the probability density function of standard operation. Moreover, the risk of missing a fault can be evaluated by the intersection between the threshold value and the probability density function of faulty state [31].

From the above description it is possible to point out that a proper design phase is needed to develop a robust and reliable diagnostic algorithm. First of all, the development of an accurate and fast numerical model allows the detection of a wide range of faulty states and the implementation of the algorithm in real-time. Then, the reliability of the FSM depends on the knowledge on the physical behaviour of each system component, as well as the number of malfunctions that can be

related to the monitored variables. Finally, the choice of threshold levels must take into account several features, such as the capability to distinguish between false alarms and missed faults, the reliability of the measurement devices available on the system plant and the model uncertainty.

The next paragraph focuses on the description of the mathematical model developed for the simulation of the SOFC system described in section 4.1.

6. SOFC MODEL

In this work a lumped-capacity model previously developed by the authors [1][2][3] has been exploited to simulate the behaviour of the SOFC system sketched in Figure 2. In the next sections a description of the main physical equations is given, but further details can be retrieved from the reference papers [1][2][3]. The hypothesis assumed for the development of the SOFC model are listed below:

- the stack is considered planar and co-flow;
- a lumped model approach is applied, without considering spatial variations;
- electrochemical reactions and mass transfer are assumed instantaneous;
- all the components are adiabatic.

Furthermore, an important aspect that must be pointed out is the necessity to develop the model not only for simulating the system behaviour in different steady-states but also during transients, in order to avoid the risk of confusing them as faulty behaviours [32].

6.1 SOFC stack

The stack is simulated by the following lumped capacity model equation:

$$K_{SOFC}\frac{dT_{SOFC,out}}{dt}=\dot{E}_{SOFC,in}\left(T_{SOFC,in}\right)-\dot{E}_{SOFC,out}\left(T_{SOFC,out}\right)-JAV_{SOFC} \quad (3)$$

in which K_{SOFC} is the stack heat capacity, $T_{SOFC,in}$ and $T_{SOFC,out}$ are the inlet and outlet stack temperatures, respectively, J is the current density, and A is the geometrical cell area. The terms $\dot{E}_{SOFC,in}(T_{SOFC,in})$ and $\dot{E}_{SOFC,out}(T_{SOFC,out})$ are the inlet and outlet energy flows, respectively, function of the stack temperatures, and V_{SOFC} is the stack voltage, evaluated through the following regression [2]:

$$V_{SOFC}=n_{cells}\left(0.1844-0.0819U_f-1.235J-0.004\lambda\frac{T_{SOFC,out}}{1000}+0.8594J\frac{T_{SOFC,out}}{1000}+0.7153\frac{T_{SOFC,in}}{1000}\right) \quad (4)$$

where n_{cells} is the number of cells, U_f is the fuel utilization and λ is the excess of air. It is worth remarking that equation (4) was obtained by curve-fitting virtual experiments, whose selection and generation were deeply described in a previous paper published by the authors [3]. In that paper, it is particularly emphasized how a hierarchical approach can be beneficial to enlarge the reference operating domain by adding operating points simulated by means of a more physical model (i.e. one dimensional), thus allowing to maximize the information content of the identification data-set. The latter is then exploited to derive the voltage black-box relationship via step-wise regression approach. In this way, the fuel cell stack can be simulated with significant reliability even in off-design conditions, thus making it possible to perform realistic faulty operation simulations.

6.2 Air blower

The air blower provides the stack with the necessary amount of air and it is the most energy consuming auxiliary device [4]. The required power is evaluated as follows:

$$P_{CMP}=\dot{m}_{air}\frac{c_p T_{air,in}}{\eta_{CMP}\cdot\eta_{EM}}\left(\beta^{\frac{k-1}{k}}-1\right) \quad (5)$$

where $T_{air,in}$ is the inlet air temperature, c_p is the specific heat at constant pressure, β is the pressure ratio, η_{EM} and η_{CMP} are the electric motor and blower efficiency, respectively, the latter being evaluated as a function of blower speed and pressure ratio through experimental efficiency maps [2]. The term $\dot{m}_{air}$ (see Eq. 5) is calculated from stoichiometry assuming a constant excess of air λ:

$$\dot{m}_{air} = \lambda \frac{n_{cells} JAM_{O_2}}{4F0.233} \tag{6}$$

6.3 Air pre-heater

According to [1] and [2], the air pre-heater has co-flow configuration and it is modelled following a zero capacity model, whose equations are described below [34]:

$$\left(K_{HE} + C_h\right)\frac{dT_{h,HE}}{dt} = \dot{E}_{h,HE,in}\left(T_{h,HE,in}\right) - \dot{E}_{h,HE,out}\left(T_{h,HE,out}\right) - U_{HE} A_{HE}\left(T_{h,HE} - T_{c,HE}\right) \tag{7}$$

$$C_c \frac{dT_{c,HE}}{dt} = \dot{E}_{c,HE,in}\left(T_{c,HE,in}\right) - \dot{E}_{c,HE,out}\left(T_{c,HE,out}\right) + U_{HE} A_{HE}\left(T_{h,HE} - T_{c,HE}\right) \tag{8}$$

The Eq. (7) refers to the hot fluid, which is the pre-reformer hot exhaust, while the equation (8) refers to the cold fluid, which represents the cathode inlet flow. K_{HE} is the solid heat capacity, whereas C_h and C_c are the heat capacities of the hot and cold gas, respectively. The term $U_{HE}A_{HE}$ is the product between the heat transfer coefficient U_{HE} and the heat exchange surface A_{HE}.

6.4 Fuel pre-reformer

As stated in [2], the fuel pre-reformer described in this work is a steam pre-reformer characterized by an evaporator and a reactor. Following the same approach used for the air pre-heater, the dynamics of both hot and cold fluid can be described by Eq. (7) and Eq. (8) respectively. The hot fluid is represented by the post-burner exhaust, whereas the cold fluid

is a mixture of methane and vapour, whose amount depends on the SOFC operating conditions. Considering a steam to carbon ratio equal to 2.5, the inlet molar flows can be computed as:

$$\dot{n}_{CH_4} = \frac{JAn_{cells}}{8FU_f} \tag{9}$$

$$\dot{n}_{H_2O} = 2.5\dot{n}_{CH_4} \tag{10}$$

6.5 Post-burner

To increase the temperature of the outlet stack gases, to be efficiently used to heat-up the inlet SOFC flows, the outlet anode gases are mixed with the cathode ones and burned into the post-burner, in which the combustion (assumed complete and adiabatic) of the residual molecules of H_2 and CO of the anode exhaust takes place [1]. The outlet temperature $T_{PB,out}$ is evaluated iteratively solving the following energy balance [1][2]:

$$\dot{E}_{PB,in}\left(T_{SOFC,out}\right) = \dot{E}_{PB,out}\left(T_{PB,out}\right) \tag{11}$$

7. SIGNATURE MATRIX IMPROVEMENT THROUGH FAULTS SIMULATION

As discussed in the previous paragraphs, the FSM presented in Table 1 was developed adopting a heuristic approach, which takes into account only qualitative relations between symptoms and faults. Indeed, the FTA connects a specific fault to several symptoms without considering their magnitude. For this reason, the direct use of the FSM as developed through a FTA may lead to a non-optimized isolation process. To be clearer, if the system is deviating from the normal behaviour, but still lying near the normal operating condition (i.e. incipient fault), some residuals move from zero, though it is not sure that they overcome the defined thresholds, due to the low magnitude of the fault. One solution could be the reduction of the thresholds levels, but, as previously stated, it could lead to an increase in the probability of false alarm. Another possibility is to use the developed model also to test the system sensitivity to different faults.

It is worth remarking that the aim of this paper is to give a guideline for the development of an improved FSM to be implemented into a comprehensive diagnostic algorithm. The study has been made with the only purpose of highlighting a plausible approach to design an improved diagnostic algorithm [32]. The considered mathematical model is exploited to reproduce both normal operating conditions and faulty states, without a specific reference to a real system and the related errors in the reproduction of the system behaviour. Since the references for the residuals evaluation are the values simulated by the model, those are deterministic in the sense that they are not associated to real measured values and the error is assumed zero. This assumption should be associated to the fact that the focus is not on the mere residual values but on the different sensitivity of the considered variables to a specific fault. A schematic representation of the guidelines of this approach is given in Figure 6.

The idea of using a model to simulate systems also during undesired states is exploited by several authors. For example, Escobet et al. [17] improved a PEFC simulator model by including sub-models, which can simulate the increment in the compressor motor friction, the compressor overheating, the air leakage in the air supply manifold and the temperature controller failure. Ingimundarson et al. [18] developed a hydrogen leakage model for a PEFC stack, whereas Simani et al. [9] proposed a turbine prototype model, which includes sub-models that simulate the compressor blades failure, the reduction of the turbine efficiency and the thermocouple sensor and controller actuator faults.

Therefore, the combination of model simulation and threshold levels definition can be helpful during both the monitoring and the FSM design. Particularly, the same model developed for the simulation of the SOFC system can be used to simulate both its normal and faulty conditions. To this purpose, the model is upgraded in such a way as to simulate the faults accounted into the FSM, at specific magnitude levels.

7.1 Faults sub-models

In the following, the description of the main equations developed to simulate the faults included into the FSM of Table 1 is given. More details can be found in Appendix A.

The fault f_1 corresponds to an increase in the air blower mechanical losses, which results in the increase in the requested electric power and in the air outlet temperature, according to Eq. (12) and Eq. (13), respectively:

$$P_{EM,F} = \frac{\dot{m}_{air} T_{air,in} c_p}{(1-\xi)\eta_{EM}\eta_{is}} \left(\beta^{(k-1)/k} - 1\right) \tag{12}$$

$$T_{CMP,out,F} = T_{air,in}\left[1 + \frac{\beta^{(k-1)/k} - 1}{\eta_{is}}\left(1 + \frac{\xi}{2(1-\xi)\eta_{EM}}\right)\right] \tag{13}$$

The coefficient ξ is related to the fault magnitude and it is limited to the range [0,1]: if the system is behaving normally (no fault) ξ is 0, whereas if the fault occurs in the system ξ is higher than 0. The fault magnitude can be expressed in percentage as $\xi \cdot 100$, and, according to Eq. (12) and Eq. (13), if ξ is equal to 1 the variables diverge (i.e. become infinite), meaning that a failure occurs and the system must be shut down.

The fault f_2 represents an air leakage between the air blower and the heat exchanger. This fault is simulated using a model of gas release through a hole (see Figure A.2), whose outlet flow is estimated as:

$$\dot{m}_H = \begin{cases} \dfrac{\pi C_D D_H^2 p_{air,out,1}}{4\sqrt{TR/M_{air}}} \left(\dfrac{p_{amb}}{p_{air,out,1}}\right)^{1/k_{air}} \sqrt{\dfrac{2k_{air}}{k_{air}-1}\left[1 - \left(\dfrac{p_{amb}}{p_{air,out,1}}\right)^{(k_{air}-1)/k_{air}}\right]} & if \quad \dfrac{p_{amb}}{p_{air,out,1}} > \left(\dfrac{2k_{air}}{k_{air}+1}\right)^{k_{air}/(k_{air}-1)} \\ \dfrac{\pi C_D D_H^2 \sqrt{k_{air}}}{4\sqrt{TR/M_{air}}} p_{air,out,1} \left(\dfrac{2}{k_{air}+1}\right)^{(k_{air}+1)/[2\cdot(k_{air}-1)]} & if \quad \dfrac{p_{amb}}{p_{air,out,1}} \le \left(\dfrac{2k_{air}}{k_{air}+1}\right)^{k_{air}/(k_{air}-1)} \end{cases} \tag{14}$$

Thus, the air amount reaching the heat exchanger is reduced by a quantity equal to $\dot{m}_H$.

The fault f_3 is related to the failure of the temperature controller. In the modelled SOFC system, the stack temperature is controlled through a feedback PI controller, which reads the stack temperature signal and acts on the regulation of the excess of air (i.e. on the air blower outlet mass flow) to keep the stack temperature within a specific range [35]. The controller fault is simulated disabling the PI controller and changing right afterwards the load value: having removed the PI controller prevent the system from adapting to the new operating condition.

The fault f_4 consists in the pre-reformer heat exchange surface corrosion. To simulate this event, the product $U_{REF}A_{REF}$, considering Eq. (7) and Eq. (8) applied to the pre-reformer, is reduced according to the following equation:

$$U_{REF,F} A_{REF,F} = U_{REF} A_{REF} (1-\chi) \tag{15}$$

where the coefficient χ has the same definition of the coefficient ξ.

The last fault (f_5) is related to the increase in the stack polarization losses, which results in a sudden decrease in the stack voltage. Such a fault is simulated hereinafter by decreasing stack voltage (see Eq. 4) by a specific amount according to the following relationship:

$$V_{SOFC,F} = V_{SOFC} (1-\varepsilon) \tag{16}$$

where ε, as ξ and χ, is a coefficient varying in the range [0,1] and it is related to the fault magnitude.

Since the purpose of the paper is to detect and isolate a fault at system level, rather than at stack level, the use of a simplified model for the stack voltage simulation is sufficient. Due to the mathematical approach here adopted, each coefficient of the mathematical regression accounts for several physical phenomena occurring in the stack, thus referring to the different polarization losses (i.e. ohmic, concentration and activation). Therefore, the introduction of a global multiplicative coefficient was considered enough suitable realistic to reproduce the effects of the considered fault.

Through the simulation of the aforementioned faults at a specific magnitude level it is possible to derive quantitative relationships linking the monitored variables variation to the fault magnitude. The SOFC system model is exploited to simulate in parallel the system both in normal and faulty conditions. First of all, with respect to the model parameters listed in Table 2, the normal values of the monitored variables are generated for two different operating conditions, with a load of 25 A and 40 A respectively (see Table 3). These values are taken as reference for the definition of the threshold values and for the evaluation of the residuals. It is worth stressing again that from each monitored variable a symptom can be derived, thus the list of monitored variables is directly linked to the list of symptoms of the FSM (see Table 1). The first operating condition (OC1 in Table 3) is taken as reference for all the faults except for the fault f_3, which is referred to the second one (OC2 in Table 3). This choice is strictly related to the simulation procedure of the fault f_3: as mentioned before, the PI is disabled and the load value is changed from 25 A to 40 A (i.e. increment of 60%). Thus, the residual must be computed referring to the operating conditions at 40 A, after the fault took place.

Afterward, the system is simulated in faulty conditions, obtaining a different set of variables values, through which the residuals can be computed. In the present case, residuals are not evaluated as shown in Eq. (1), but they are computed as relative values, as follows:

$$r = \frac{\left|Y - \hat{Y}\right|}{\hat{Y}} \cdot 100 \tag{17}$$

This gives for each monitored variable a uniform evaluation of the deviation from the normal conditions and the same choice of the thresholds values. Indeed, the thresholds are defined as a percentage of the normal variables values, which in turn depend on the current operating condition. Thus, instead of fixed thresholds, the authors assumed variable thresholds according to the current operating status.

8. RESULTS AND DISCUSSIONS

The faults described in the previous paragraph have been simulated assuming a fault magnitude of about 10%. For example, referring to the air leakage fault, the hole diameter size is set to 2.5 mm, which corresponds to an outlet mass flow through the hole of 2.526 kg/h, whereas air flow in normal operation equals 23.126 kg/h (see Table 3). With this diameter value, the leakage roughly corresponds to the 10% of the air mass flowing in normal conditions. The only exception is made for the simulation of fault f_4, choosing a 50% magnitude size. The reasons for this assumption are explained in the following.

Five simulations have been performed to reproduce the occurrence of all the considered faults, due to the hypothesis that only one fault at a time can occur in the system. This assumption is considered since the purpose of this work is to understand the effects of each fault on the entire system. Indeed, considering one or more faults happening simultaneously can induce cumulative effects which hinders a univocal fault isolation, which is the chief objective of the work.

As an example, to simulate the increase in the air blower mechanical losses, the fault coefficient ξ is raised from 0 to 0.1. This value may correspond to an incipient fault (i.e. magnitude of 10%). The effects consist in the increase in the blower power and in the temperature at the blower outlet, as expected from equations (12) and (13), herein presented in Figure 7. From Figure 7-a it is possible to notice that, when the fault occurs at 2500 s, the blower power suddenly diverges from 0.4692 kW, reaching at steady state a value of 0.5223 kW (i.e. a variation of about 11.3%). On the other hand, the

outlet temperature variation reported in Figure 7-b, consists in a rapid growth from 85.68°C to 89.42°C, corresponding to a variation of around 1% (evaluated in Kelvin) at steady state.

Another example is here presented with respect to the simulation of the pre-reformer heat exchange surface corrosion. This fault is simulated reducing the characteristic pre-reformer surface according to equation (15). This event directly affects the pre-reformer outlet cold fluid temperature (see equation (8)), used as the reference pre-reformer temperature for the computation of the outlet fuel composition. The fault coefficient χ is risen from 0 to 0.5 at 2500 s, causing a reduction in the pre-reformer temperature to 604.41°C (Figure 8-a), which is about 9.8% less than the reference temperature (see Table 3). This reduction causes a variation into the outlet fuel composition, as showed in Figure 8-b, where the hydrogen molar flow variation is depicted.

The simulation results of all the considered faults in terms of residuals are presented in Figure 9 where each chart represents the residuals values (blue bars) computed through Eq. (17), after reaching a steady-state condition during the simulation process. On the *x* axes the numbers of each monitored variable are listed with reference to the order followed in Table 3. In this figure are also sketched two threshold values, fixed respectively to 1% and 5% of the values attained by each variable during normal operations (the first in red straight-dot line and the second in green dashed line respectively). The 1% threshold is assumed in order to highlight the minimum influence on certain variables, whereas the 5% threshold is then introduced to remark the effects on the diagnosis accuracy when setting a different level. Actually, when facing real system applications, the threshold choice is strictly related to the model accuracy, the resolution of the available measurement devices and the measurement noise. Moreover, the choice of the optimal threshold level should be a compromise between the capability of detecting incipient faults and reducing the probability of false alarms (see Figure 5). The symptoms' vectors computed for each threshold value are collected in the Modified Fault Signature Matrixes (MFSMs) of Table 4 and Table 5.

The two MFSMs are compared with the FSM of Table 1 and the differences with respect to the symptoms' vectors of the FSM are highlighted in Table 4 and Table 5 using a grey background colour for the cells of the vectors. As a first remark, from Table 4 it can be asserted that, referring to those of the FSM of Table 1, two fault patterns (i.e. f_2 and f_4) are kept unchanged, whereas, in the MFSM of Table 5, at least one symptom is changed.

For fault f_1 (air blower) it is possible to point out that the modification in the MFSM of Table 4 occurs only to the symptom s_{10} (air temperature at cathode inlet), which is no more involved in the isolation process of this specific fault (i.e. is changed from 1 to 0). The motivation for this discrepancy resides in the small increment in the air flow (about 0.048 kg/h, barely visible in Figure 9 – symptom s_{12}) induced by the controller to keep the stack temperature near the set-point. This

increment leads to the compensation of the temperature at the blower outlet, which could induce, in uncontrolled condition, an increase in the stack temperature. On the other hand, the symptoms' vector related to a threshold level of 5%, presented in Table 5, differs from the one of the starting FSM of Table 1 not only in the air temperature at cathode inlet (symptom s_{10}), as for the previous one, but also in the net electric power (symptom s_3) and the temperature at the blower outlet (symptom s_8), all changing from 1 to 0. However, this variation is motivated by the small residuals values of the aforementioned variables, which are all lower than 5%.

The symptoms' vector related to fault f_2 (air leakage) does not present any variation with a threshold level of 1%, whereas for a threshold level of 5% the MFSM shows just one different symptom (i.e. the net power – symptom s_3 – switches from 1 to 0). Indeed, the percent variation of the net electric power is about 1.9%, thus triggering a symptom only for the 1% threshold value.

As mentioned before, the temperature controller failure does not require a specific sub-model, but it is induced by switching off the PI controller at a certain time and changing afterwards the required current. In this case, the detection of the fault is performed comparing the variables values obtained after the controller switch off to their expected values (i.e. obtained with the controller switched on) at the new operating condition. In this way, the controller failure can be identified considering the different adaptation of the monitored values. In the specific case, the load is changed from 25 A (i.e. OC1) to 40 A (i.e. OC2) and the variables values related to each operating condition are listed in Table 3. In this case, the presented results cannot be related to a specific fault magnitude because of the binary nature of the fault, i.e. the PI controller can be either on or off. For this reason, the amplification of the effects can only be affected by the current step change. From Figure 9, we can observe that all the residuals but two diverge from zero. This behaviour leads to the two symptoms' vectors presented one in Table 4 for a threshold of 1% and one in Table 5 for a threshold of 5%. What emerges from the comparison of these symptoms vectors to that of the starting FMS of Table 1 is that both the two new symptoms' vectors show several discrepancies. First of all, the fuel temperature at anode inlet (symptom s_6) becomes 0 in both cases. This difference is due to its residual value lower than 1% (see Figure 9). However, the substantial differences belong to the blower power (symptom s_2), the excess of air (symptom s_5) and the air mass flow at cathode inlet (symptom s_{12}), which become all 1. The explanation of these changes resides in the controller fault simulation process. Compared to the detection based on the FTA of Arsie et al. [4], the simulation entails a current demand variation, which is not considered by the FTA in [4]. The other differences, showed only by the symptoms' vector for a 5% threshold, are due to the related low residuals values.

As observed for the fault f_3, also the symptoms' vectors related to the fault f_4 show several discrepancies. What is important to remark is that the magnitude used to simulate this fault was set to 50%, due to the low influence of the fault on the related variables, as can be observed from Figure 9. Concerning the symptom vector for a threshold level of 1%, four symptoms change from 1 to 0: the blower power (symptom s_2), the excess of air (symptom s_5), the post-burner exhaust temperature (symptom s_7) and the air mass at cathode inlet (symptom s_{12}). However, the main significant difference resides in the post-burner exhaust temperature. Indeed, this variable seems not to be affected by this fault. The other symptoms changes are all due to the related low residuals values. The same conclusions can be extended also to the symptoms' vector for a 5% threshold, which shows five more symptoms being zeroed.

Finally, the symptoms' vector for the fault f_5 in Table 4 is exactly the same of the one in Table 1, whereas the symptoms' vector in Table 5 differs from this latter by four symptoms, which are changed from 1 to 0, due to the small residual values compared to a 5% threshold.

On the basis of the above results, the first observation which can be made on the FSM of Table 4 is that all the rows are different from each other, allowing the univocal identification of the considered faults, which cannot be performed with the starting FSM of Table 1. Furthermore, only two rows are rather modified (fault f_3 and fault f_4), whereas other two are kept unchanged (fault f_2 and fault f_5). On the other hand, the FSM of Table 5 is quite different from the starting FSM of Table 1, since all the rows have been changed. Only one row (fault f_2) has only one symptom changed, whereas all the others present at least three different symptoms values. Moreover, the rows associated to the faults f_1 and f_2 present the same pattern hindering the possibility to exploit this FSM for an univocal isolation process.

To deepen the effects of the operating conditions on the MFSMs development, all the faults considered in this work have been analysed also with respect to the operating condition OC2, with a current load set to 40 A (see Table 3). Under the hypothesis of one fault occurring at a time, a fault magnitude of about 10% has been considered for faults f_1, f_2 and f_5, whereas a fault magnitude of 50% has been considered for fault f_4, according to the same motivations previously depicted. Fault f_3 has been simulated imposing a change of operating condition from OC2 to OC1, thus referring the obtained residuals to this latter operating condition. The results of the simulated residuals are presented in Figure 10. From the analysis of this figure, it is possible to observe that a change in the operating condition does not evidently affect the residual sizes, and in turn the MFSMs design. Indeed, assuming a 5% threshold, the same MFSM of Table 5 is obtained. On the other hand, if a 1% threshold is assumed, slight modifications in the MFSM occur. With respect to the MFSM presented in Table 4, three symptoms become 0: for fault f_1, the air temperature at compressor outlet (symptom s_8); for fault f_5, the fuel temperature at anode inlet (symptom s_6) and the hot fluid temperature at air pre-heater inlet (symptom s_9). This symptoms

change is caused by the slight reduction in the residuals sizes, that are all below 1%. As an example, the residual related to symptom s_8 for the fault f_1 has a size of 0.99% with a fault magnitude of 10%. Although near the threshold, this value does not trigger the related symptom, hindering an univocal isolation process with the obtained MFSM. Indeed, the symptoms' vector of fault f_1 is in this case the same of fault f_2 (as for the MFSM of Table 5 for OC1). This result underlines the need for setting a proper threshold value during the MFSMs design, which should take into account, on one hand, the accuracy of the model and the available measurement devices and, on the other hand, also the working conditions in which an SOFC system can operate.

Concerning the effects of the fault magnitude, it is worth noting that the purpose of the present paper is to give a detailed description of the design procedure of a Fault Signature Matrix with main focus on incipient faults (i.e. with low magnitude). As already observed for fault f_4 at OC1, a small fault magnitude does not induce a significant variation in the residuals values, triggering few symptoms even though with a 1% threshold level. As an example, with a magnitude of 10%, the simulation of fault f_4 leads just one symptom (i.e. symptom s_6) to hardly overcome the 1% threshold level (see Figure 11). Indeed, its residual value is about 1.25%. Accordingly, small magnitude faults lead to a MFSM with mainly zeros. On the other hand, high magnitude faults lead to the opposite effect. In Figure 12, the residuals simulated with a fault magnitude at 50% are sketched. The comparison of these residuals with two threshold levels gives the MFSMs presented in Table 6 and Table 7, for 1% and 5% thresholds respectively. In these Tables, the modifications with respect to the FSM of Table 1 are highlighted using a grey background colour for the cells of the vectors, whereas the differences with the MFSMs of Table 4 and Table 5 are highlighted using black bold edges. Comparing the MFSM of Table 4 with that of Table 6, the latter shows three more symptoms becoming 1 with respect to the former. In the specific, symptoms s_5 and s_{12} are triggered for fault f_1, whereas, symptom s_8 becomes one for fault f_2. Nevertheless, comparing the MFSM of Table 7 with the one of Table 5, six symptoms differ: for fault f_1, symptoms s_3 and s_8 become one; for fault f_2, only the symptom s_3 is further triggered; finally, for fault f_5, symptoms s_6, s_7 and s_{10} become active. It is worth noting that both the MFSMs of table 6 and table 7 can be used for an univocal isolation of the proposed faults. According to this result, it is possible to point out that, considering a higher fault magnitude, the overlapping of the symptoms' vectors related to faults f_1 and f_2 with a threshold level of 5% (see Table 5) can be avoided. However, rising the magnitude of the considered faults during the MFSM design process hinders the capability of detecting incipient faults, increasing the risk of system damage and performance losses when applied.

After these comments some general remarks arise. First of all, it is worth recalling that the FSM was built via fault tree analysis, whereas the MFSMs were built by exploiting an SOFC system model with embedded faults simulations. The

former signature matrix building process depends on the available system knowledge and on the experience brought from either literature or on-field data. A lack of knowledge on the faulty processes as well as the difficulties of accounting multiple phenomena affecting each fault may limit the achievement of an effective fault isolation. On the other hand, the model-based FSM building process can enhance the fault isolation by introducing quantitative analysis. Moreover, complex non-linear interactions among processes are accounted for and, thus, a more complete study on the occurrence of each fault can be developed. Therefore, the design of any diagnosis tool can be accomplished with less experimental resources and in a more systemic way. As seen before, another advantage of the model-based approach is the possibility to solve the compromise among detection capability, number of measurement devices, risk of false alarm and misdetection, which are strategic issues in FDI algorithm design and implementation. However, developers must be aware of some problems that may arise when using models with low accuracy or poor fault process description. Another general remark has to be reported about the sensitivity of the isolation process with respect to the residuals generated when a fault occurs. It has been discussed above that a threshold below 5% has to be set to detect faults whose occurrence affect the performance of the faulty sub-system by 10%; this means that a sort of damping or a loss of information brought from the signal occurs in the detection process. Therefore, an improvement of the detection capability has to be considered to increase the sensitivity of the fault isolation process. Since the amount of derivable information depends on the number of installed measuring devices, one way to increase the sensitivity is to probe the input variables (both control and exogenous) and derive from them other features (i.e. residuals). Such an approach [21] may be awkward to implement because the monitoring model must reproduce the inverse process, which –in a more general sense– entails simulating the inputs as a function of the outputs. These aspects have to be considered when implementing new SOFC system diagnosis with improved faults isolation capabilities.

9. CONCLUSIONS

In this paper the design of a methodology to support the development of a diagnosis algorithm for Solid Oxide Fuel Cell (SOFC) systems has been presented. Basically, the fault isolation task has been addressed in the paper. This part of the diagnosis design process represents the main issue to be solved during diagnostic algorithm development. A model-based approach relying on the simulation of both normal and faulty behaviour of a monitored SOFC system has been described. The model is based on a dynamic (lumped) model developed in [1][2][3], which is enhanced by including further sub-models for the simulation of five faults at system level. The faults simulation is useful to generate a robust reference

database, implemented during the isolation process. The first version of the initial reference information (i.e. Fault Signature Matrix – FSM) has been derived from the Fault Tree Analysis (FTA) performed by the authors in [4] and has been obtained through a heuristic approach, which takes into account only qualitative links between symptoms and faults. To implement a quantitative process, the mathematical model has been considered to simulate all the faults in a new FSM. For each fault, two threshold values has been considered at 1% and 5% of the normal operating values, respectively. Each threshold level led to a specific symptoms' vector and this latter has been then compared to the FSM symptom vector of the same fault. Two different Modified Fault Signature Matrices (MFSMs) have been obtained and can be exploited for the diagnosis algorithm implementation. The influence of changing the operating conditions and the faults magnitude on the MFSMs development has been also investigated.

ACKNOWLEDGEMENTES

This work was carried out in the framework of the project GENIUS (Generic diagnosis instrument for SOFC systems) and the research leading to these results has received funding from the European Community's Seventh Framework Programme (FP7/2007-2013) for the Fuel Cells and Hydrogen Joint Technology Initiative under grant agreement n° 245128 and from the University of Salerno (project FARB 2010).

REFERENCES

[1] M. Sorrentino, C. Pianese, J. Power Sources 196 (2011) 9036-9045.

[2] M. Sorrentino, C. Pianese, J. Fuel Cell Sci. and Technol. 6 (2009), 041011/1-041011/12.

[3] M. Sorrentino, C. Pianese, Y.G. Guezennec, J. Power Sources 180 (2008) 380-392.

[4] I. Arsie, A. Di Filippi, D. Marra, C. Pianese, M. Sorrentino, Proceedings of the ASME 2010 Eighth International Fuel Cell Science, Engineering and Technology Conference, FuelCell2010, June 14-16, 2010, Brooklyn, New York, USA.

[5] Q. Huang, R. Hui, B. Wang, J. Zhang, Electrochem. Acta 52 (2007) 8144-8164.

[6] C.S. Singhal , K. Kendell, High Temperature Solid Oxide Fuel Cells: Fundamentals, Design and Applications, Elsevier Ltd., Oxford, UK, 2004.

[7] J.J. Botti, M.J. Grieve, J.A. MacBain, SAE Paper No. 2005-01-1172, 2005.

[8] R. Isermann, Annu. Rev. Control 29 (2005) 71-85.

[9] S. Simani, C. Fantuzzi, Mechatron. 16 (2006) 341-363.

[10] K. Wang, D. Hissel, M.C. Pera, N. Steiner, D. Marra, M. Sorrentino, C. Pianese, M. Monteverde, P. Cardone, J. Saarinen, Int. J. Hydrogen Energy 36 (2011) 7212-7228.

[11] L. Barelli, G. Bidini, A. Ottaviano, Appl. Energy 110 (2013) 173–189.

[12] A.S. Martinez, J. Brouwer, G.S. Samuelsen, J. Power Sources 213 (2012) 203-217.

[13] S.A. Hajimolana, M.A. Hussain, W:M:A: Wan Daud, M.H. Chakrabarti, Chem. Eng. Res. Des. 90 (2012) 1871–1882.

[14] F. Arpino, M. Dell'Isola, D. Maugeri, N. Massarotti, A. Mauro, Int. J. Hydrogen Energy 38 (2013) 336-344.

[15] L. Barelli, G. Bidini, F. Gallorini, P.A. Ottaviano, Int. J. Hydrogen Energy 38 (2013) 354-369.

[16] D. Marra, C. Pianese, M. Sorrentino (2011), ASME 2011 9th International Conference on Fuel Cell Science, Engineering and Technology, August 7-10, Washington, DC, USA, 2011. ASME proceedings, pp. 449-455 January 01, 2011, doi: 10.1115/FuelCell2011-54686.

[17] T. Escobet, D. Feroldi, S. De Lira, V. Puig, J. Quevedo, J. Riera, M. Serra, J. Power Sources 192 (2009) 216-223.

[18] A. Ingimundarson, A.G. Stefanopoulou, D. McKay, IEEE Trans. Control Syst. Technol. Vol. 16 No. 5 (2008) 1004-1012.

[19] N. Fouquet, C. Doulet, C. Nouillant, G. Dauphin-Tanguy, B. Ould-Bouamama, J. Power Sources 159 (2006) 905-913.

[20] F. Kimmich, A. Schwarte, R. Isermann, Control Eng. Pract. 13 (2005) 189-203.

[21] Y. Kim, G. Rizzoni, V. Utkin, IEEE Control Syst. Vol.18 (1998) 84-99.

[22] A.C. Leite, R.V. Da Fonseca Lopes, H.K. Kuga, Brazilian Conference on Dynamics, Control and Their Applications DINCON 2006, May 22 – 26, Guaratinguetà, SP, Brazil, 2006.

[23] C.H. Lo, Y.K. Wong, A.B. Rad, ISA Transaction 43 (2004) 459-475.

[24] M. Chantler, A. Aldea, Eng. Appl. Artif. Intell. 11 (1998) 135-148.

[25] Y. Papadopoulos, Reliab. Eng. Syst. Saf. 81 (2003) 325-341.

[26] P. Frank, E.A. García, B. Köppen-Selinger, Math. Comput. Simul. 53 (2000) 259-271.

[27] R. Isermann, Fault-Diagnosis Systems, An Introduction from Fault Detection to Fault Tolerance, Springer, New York, 2006.

[28] M. Witczak, Identification and Fault Detection of Non-Linear Dynamic Systems, University of Zielona Gora Press, Poland, 2003.

[29] M. Sorrentino M., Development of a Hierarchical Structure of Models for Simulation and Control of Planar Solid Oxide Fuel Cells, Ph.D. Thesis, University of Salerno, Italy, 2005.

[30] S. Zhang, X. Yuan, H. Wang, W. Mérida, H. Zhu, J. Shen, S. Wu, J. Zhang, Int. J. Hydrogen Energy 34 (2009) 388-404.

[31] I. Arsie, G. Flauti, C. Pianese, G. Rizzo, C. Barberio, R. Flora, G. Serra, C. Siviero, Proceedings of the SYSID 2000 IFAC Symposium on System Identification (2000) 137–142.

[32] F.D. McKenzie, A.J. Gonzales, R. Morris, Eng. Appl. Artif. Intell. 11 (1998) 279-291.

[33] W.E. Veseley, Fault Tree Handbook, Systems and Reliability Research, Office of Nuclear Regulatory Research, U.S. Nuclear Regulatory Commission, Washington, D.C, USA, 1981.

[34] O.E. Ataer, A. Ileri, Y. Gogus, Int. J. Refrig. Vol. 18 No. 3 (1995) 153-160.

[35] P. Aguiar, C.S. Adjiman , N.P. Brandon, J. Power Soures 147 (2005) 163-147.

[36] R.B. Bird, W.E. Stewart, E.N. Lightfoot, Transport Phenomena, J. Wiley & Sons, New York, 1960.

[37] Yuhu D., Huilin G., Jing'en Z., Yaorong F., Chem. Eng. J. 92 (2003) 237–241.

[38] D. Yuhua, G. Huilin, Z. Jing'en, F. Yaorong, J. Loss Prevention in the Process Ind. 15 (2002) 423–428.

[39] A. Sorce, A. Greco, L. Magistri, P. Costamagna, Applied Energy 136 (2014) 894–908.

[40] L. Barelli, E. Barluzzi, G. Bidini, Int. J. Hydrogen Energy 38 (2013) 5060-5074.

[41] Ph. Hofmann, K.D. Panopoulos, J. Power Sources 195 (2010) 5320–5339.

[42] J.I. Gazzarri, O. Kesler, J. Power Sources 167 (2007) 100–110.

[43] D. Marra, M. Sorrentino, Cesare Pianese, B. Iwanschitz, J. Power Sources 241 (2013) 320-329

[44] M. Sorrentino, D. Marra, C. Pianese, M. Guida, F. Postiglione, K. Wang, A. Pohjoranta, Energy Procedia 45 (2014) 298–307.

[45] R. Shirkhani, H. Jazayeri-Rad, S. J. Hashemi, J. Natural Gas Science and Engineering 21 (2014) 1171-1183.

[46] U. K. Chakraborty, Energy 34 (2009) 740–751.

[47] J. Milewski, K. Swirski, Int. J. Hydrogen Energy 34 (2009) 5546 – 5553.

[48] GENIUS project (GEneric diagNosis Instrument for SOFC systems), European Union's Seventh Framework Programme (FP7/2007-2013) for the Fuel Cells and Hydrogen Joint Technology Initiative, grant agreement n° 245128 – website: https://genius.eifer.uni-karlsruhe.de

APPENDIX A

A.1 Fault f_1: Air Blower Fault

The fault considered for the air blower consists of an increase in the mechanical losses, which leads to an upsurge of the compressor absorbed power and outlet temperature. In normal conditions, from the definition of the mechanical efficiency η_{EM} it is possible to define the absorbed power as function of the compressor power as:

$$P_{EM} = \frac{P_{CMP}}{\eta_{EM}} = \frac{\dot{m}_{air} T_{air,in} c_p}{\eta_{EM}\eta_{is}} \left(\beta^{(k-1)/k} - 1\right) \tag{A.1}$$

where $\dot{m}_{cmp}$ is the compressor mass flow, $T_{cmp,in}$ is the compressor inlet temperature, c_p is the specific heat capacity at constant pressure, η_{is} is the isentropic efficiency and β is the pressure ratio. Instead, the outlet temperature $T_{cmp,out}$ can be evaluated as:

$$T_{CMP,out} = T_{air,in}\left[1 + \frac{1}{\eta_{is}}\left(\beta^{(k-1)/k} - 1\right)\right] \tag{A.2}$$

When the fault occurs in the system, the mechanical efficiency decreases according to the following law:

$$\eta_{EM,F} = \eta_{EM}(1-\xi) \tag{A.3}$$

where ξ is a coefficient limited into the range [0,1]. Thus, the absorbed power in faulty condition is:

$$P_{EM,F} = \frac{P_{CMP}}{\eta_{EM,F}} = \frac{\dot{m}_{air} T_{air,in} c_p}{(1-\xi)\eta_{EM}\eta_{is}} \left(\beta^{(k-1)/k} - 1\right) = \frac{P_{EM}}{(1-\xi)} \tag{A.4}$$

The power increment compared with that in normal condition can be considered as a thermal loss Q:

$$Q = P_{EM,F} - P_{EM} = \frac{P_{EM}}{(1-\xi)} - P_{EM} = P_{EM}\frac{\xi}{(1-\xi)} \tag{A.5}$$

To define the outlet temperature in faulty condition the following assumption is made: a fraction of this thermal loss (i.e. 50%) is transmitted to the fluid as thermal power. Thus, it is possible to write:

$$\frac{Q}{2} = \dot{m}_{air} c_p \left(T_{CMP,out,F} - T_{CMP,out}\right) \tag{A.6}$$

and the outlet temperature in faulty condition is:

$$\begin{aligned} T_{CMP,out,F} &= T_{CMP,out} + \frac{Q}{2\dot{m}_{air} c_p} = T_{air,in}\left[1 + \frac{1}{\eta_{is}}\left(\beta^{(k-1)/k} - 1\right)\right] + \frac{P_{EM}}{2\dot{m}_{air} c_p}\frac{\xi}{(1-\xi)} = \\ &= T_{air,in}\left[1 + \frac{1}{\eta_{is}}\left(\beta^{(k-1)/k} - 1\right)\right] + \frac{T_{air,in}}{2\eta_{EM}\eta_{is}}\left(\beta^{(k-1)/k} - 1\right)\frac{\xi}{(1-\xi)} = \\ &= T_{air,in}\left[1 + \frac{\beta^{(k-1)/k} - 1}{\eta_{is}}\left(1 + \frac{\xi}{2(1-\xi)\eta_{EM}}\right)\right] \end{aligned} \tag{A.7}$$

A.2 *Fault f_2: Air leakage between air compressor and pre-heater*

The connection between the air blower and the air pre-heater is guaranteed through the utilization of a pipe, which is assumed horizontal and with constant section (Figure A.1). In this figure the subscript air is neglected. Furthermore, the gas is considered perfect and all the heat exchanges between the pipe and the ambient are neglected (i.e. the pipe and the gas are considered isothermal). All these assumptions are fundamental for the purpose of reducing the computational burden. Considering the pipe of Figure A.1, the mass conservation equations can be written as follows:

$$\dot{m}_{air,in} = \dot{m}_{air,out} = \dot{m} = const. \tag{A.8}$$

Accounting that for all the following equations the considered gas is air, all the subscripts will be written without the statement *air*. Under the assumption of constant section, the Eq. (A.8) becomes:

$$\rho_{in} v_{in} = \rho_{out} v_{out} = \rho v = const. \tag{A.9}$$

where v is the straight velocity (i.e. the component of vector in the direction of the flow – perpendicular to the pipe section). Differentiating the Eq. (A.9):

$$\frac{d\rho}{\rho} = -\frac{dv}{v} \tag{A.10}$$

and the gas state equation in isothermal conditions:

$$\frac{dp}{p} = \frac{d\rho}{\rho} \tag{A.11}$$

and combining the Eq. (A.10) and Eq. (A.11) together, the following equation can be carried out:

$$\frac{dp}{p} = -\frac{dv}{v} \Rightarrow dv = -v\frac{dp}{p} \Rightarrow vdv = -v^2\frac{dp}{p} \tag{A. 12}$$

Considering the mechanical energy equation in differential form (neglecting the height difference between pipe inlet and outlet):

$$\frac{dp}{\rho} + vdv + \frac{f}{2D}v^2 dx = 0 \tag{A. 13}$$

where the last term corresponds to the friction losses, it is possible to substitute the Eq. (A.12) into the Eq. (A.13), obtaining:

$$\frac{dp}{\rho} - v^2 \frac{dp}{p} + \frac{f}{2D} v^2 dx = 0 \tag{A. 14}$$

Taking into account the perfect gas equation, the Eq. (A.14) can be written as:

$$\frac{1}{RT(v\rho)^2} p dp - \frac{dp}{p} + \frac{f}{2D} dx = 0 \tag{A. 15}$$

Integrating the Eq. (A.15) on the entire pipe length:

$$\frac{\left(p_{out}^2 - p_{in}^2\right)}{2RT(v\rho)^2} - \log\left(\frac{p_{out}}{p_{in}}\right) + \frac{f}{2D} L = 0 \tag{A. 16}$$

With further mathematical passages, Eq. (A.16) can be written as [35]:

$$\overline{R} \frac{\pi^2}{32} \left(\frac{\rho_{air,in}^2 T D^4}{\dot{m}_{air,in}^2 M_{air}}\right) \left[\left(\frac{p_{air,out}}{p_{air,in}}\right)^2 - 1\right] - \ln\left(\frac{p_{air,out}}{p_{air,in}}\right) + \frac{f}{2}\left(\frac{L}{D}\right) = 0 \tag{A. 17}$$

through which the outlet air pressure can be calculated, upon the knowledge of the pipe length L and diameter D and the air input conditions (i.e. density $\rho_{air,in}$, mass flow $\dot{m}_{air,in}$ and inlet pressure $p_{air,in}$).

The air leakage can be simulated through the introduction of a hole with diameter D_H, as sketched in Figure A.2. In this figure it is possible to identify three main control volume: the volumes 1 and 2, whose outlet properties are easily calculated through Eq. (A.8) and Eq. (A.17), and the middle volume of length D_H, where the hole is located. The mass balance in this latter control volume can be written as:

$$\dot{m}_{air,in,2} = \dot{m}_{air,out,1} - \dot{m}_H \tag{A. 18}$$

where $\dot{m}_H$ is the hole outlet flow, which can be calculated according to [34] and [38] using nozzle equations in choked and un-choked flows. To distinguish between these two different conditions, the Critical Pressure Ratio (CPR) must be considered:

$$CPR = \frac{p_{amb}}{p_c} = \left(\frac{2k_{air}}{k_{air}+1} \right)^{k_{air}/(k_{air}-1)} \tag{A. 19}$$

When $p_{amb}/p_{air,out,1} > CPR$ the flow is subsonic (un-choked condition) and the outlet flow can be modelled as:

$$\dot{m}_H = \frac{\pi C_D D_H^2}{4\sqrt{T\overline{R}/M_{air}}} p_{air,out,1} \left(\frac{p_{amb}}{p_{air,out,1}} \right)^{1/k_{air}} \sqrt{\frac{2k_{air}}{k_{air}-1} \left[1 - \left(\frac{p_{amb}}{p_{air,out,1}} \right)^{(k_{air}-1)/k_{air}} \right]} \tag{A. 20}$$

while, if $p_{amb}/p_{air,out,1} \leq CPR$, the flow is sonic (choked condition) and the outlet flow is computed as:

$$\dot{m}_H = \frac{\pi C_D D_H^2 \sqrt{k_{air}}}{4\sqrt{T\overline{R}/M_{air}}} p_{air,out,1} \left(\frac{2}{k_{air}+1} \right)^{(k_{air}+1)/[2\cdot(k_{air}-1)]} \tag{A. 21}$$

To evaluate the air properties after the hole, the assumption of a constant velocity is made (i.e. $v_{air,out,1} = v_{air,in,2}$).

LIST OF TABLES

	Symptoms	Stack power	Compressor power	Net power	Stack temperature	Excess of air	Fuel temperature at anode inlet	Post burner exhaust temperature	Air temperature at compressor outlet	Hot fluid temperature at air pre-heater inlet	Air temperature at cathode inlet	Stack voltage	Air mass at cathode inlet	Temperature at anode outlet	Air temperature at cathode outlet
Faults		s_1	s_2	s_3	s_4	s_5	s_6	s_7	s_8	s_9	s_{10}	s_{11}	s_{12}	s_{13}	s_{14}
Air blower fault	f_1	0	1	1	0	0	0	0	1	0	1	0	0	0	0
Air leakage between air compressor and pre-heater	f_2	0	1	1	0	0	0	0	0	0	0	0	0	0	0
Temperature controller failure	f_3	1	0	1	1	0	1	1	0	1	1	1	0	1	1
Pre-reformer fault	f_4	1	1	1	0	1	1	1	0	1	1	1	1	0	0
Stack fault	f_5	1	1	1	0	1	1	1	0	1	1	1	1	0	0

MODEL PARAMETER	UNIT	VALUE
Geometrical cell area A	cm^2	100
Cells number n_{cells}	-	150
Stack heat capacity K_{SOFC}	$J\ K^{-1}$	8234
Fuel utilization U_f	-	0.7
Inlet air temperature $T_{air,in}$	°C	25
Inlet air pressure p_{amb}	Pa	10^5
Blower pressure ratio β	-	1.3
Electric motor efficiency η_{EM}	-	0.9
Pre-heater heat exchanger transfer coefficient U_{HE}	$W\ m^{-2}\ K^{-1}$	200
Pre-heater heat exchange area A_{HE}	m^2	0.3
Pre-heater heat capacity K_{HE}	$J\ K^{-1}$	316
Reformer heat exchanger transfer coefficient U_{REF}	$W\ m^{-2}\ K^{-1}$	200
Reformer heat exchange area A_{REF}	m^2	0.06
Reformer heat capacity K_{REF}	$J\ K^{-1}$	59

#	MONITORED VARIABLE	UNIT	OC1	OC2
1	Stack power	kW	2.895	4.3095
2	Compressor power	kW	0.4692	0.7696
3	Net power	kW	2.4263	3.5399
4	Stack Temperature	°C	825.00	825.00
5	Excess of air	-	4.8124	5.1908
6	Fuel temperature at anode inlet	°C	700.01	707.64
7	Post burner exhaust temperature	°C	1065.6	1050.2
8	Air temperature at compressor outlet	°C	85.68	82.68
9	Hot fluid temperature at air pre-heater inlet	°C	862.32	856.28
10	Air temperature at cathode inlet	°C	700.22	683.63
11	Current density	$A\ cm^{-2}$	0.25	0.40
12	Stack voltage	V	115.82	107.74
13	Air mass at cathode inlet	$kg\ h^{-1}$	23.126	39.911
14	Temperature at anode outlet	°C	825.00	825.00
15	Air temperature at cathode outlet	°C	825.00	825.00

Symptoms / Faults		Stack power	Compressor power	Net power	Stack temperature	Excess of air	Fuel temperature at anode inlet	Post burner exhaust temperature	Air temperature at compressor outlet	Hot fluid temperature at air pre-heater inlet	Air temperature at cathode inlet	Stack voltage	Air mass at cathode inlet	Temperature at anode outlet	Air temperature at cathode outlet
Faults		s_1	s_2	s_3	s_4	s_5	s_6	s_7	s_8	s_9	s_{10}	s_{11}	s_{12}	s_{13}	s_{14}
Air blower fault	f_1	0	1	1	0	0	0	0	1	0	0	0	0	0	0
Air leakage between air compressor and pre-heater	f_2	0	1	1	0	0	0	0	0	0	0	0	0	0	0
Temperature controller failure	f_3	1	1	1	1	1	0	1	0	1	1	1	1	1	1
Pre-reformer fault	f_4	1	0	1	0	0	1	0	0	1	1	1	0	0	0
Stack fault	f_5	1	1	1	0	1	1	1	0	1	1	1	1	0	0

Symptoms / Faults		Stack power	Compressor power	Net power	Stack temperature	Excess of air	Fuel temperature at anode inlet	Post burner exhaust temperature	Air temperature at compressor outlet	Hot fluid temperature at air pre-heater inlet	Air temperature at cathode inlet	Stack voltage	Air mass at cathode inlet	Temperature at anode outlet	Air temperature at cathode outlet
Faults		s_1	s_2	s_3	s_4	s_5	s_6	s_7	s_8	s_9	s_{10}	s_{11}	s_{12}	s_{13}	s_{14}
Air blower fault	f_1	0	1	0	0	0	0	0	0	0	0	0	0	0	0
Air leakage between air compressor and pre-heater	f_2	0	1	0	0	0	0	0	0	0	0	0	0	0	0
Temperature controller failure	f_3	0	1	1	0	1	0	0	0	0	0	0	1	0	0
Pre-reformer fault	f_4	0	0	0	0	0	1	0	0	0	0	0	0	0	0
Stack fault	f_5	1	1	1	0	1	0	0	0	0	0	1	1	0	0

Symptoms / Faults		Stack power	Compressor power	Net power	Stack temperature	Excess of air	Fuel temperature at anode inlet	Post burner exhaust temperature	Air temperature at compressor outlet	Hot fluid temperature at air pre-heater inlet	Air temperature at cathode inlet	Stack voltage	Air mass at cathode inlet	Temperature at anode outlet	Air temperature at cathode outlet
Faults		s_1	s_2	s_3	s_4	s_5	s_6	s_7	s_8	s_9	s_{10}	s_{11}	s_{12}	s_{13}	s_{14}
Air blower fault	f_1	0	1	1	0	1	0	0	1	0	0	0	1	0	0
Air leakage between air compressor and pre-heater	f_2	0	1	1	0	0	0	0	1	0	0	0	0	0	0
Temperature controller failure	f_3	1	1	1	1	1	0	1	0	1	1	1	1	1	1
Pre-reformer fault	f_4	1	0	1	0	0	1	0	0	1	1	1	0	0	0
Stack fault	f_5	1	1	1	0	1	1	1	0	1	1	1	1	0	0

Symptoms / Faults		Stack power	Compressor power	Net power	Stack temperature	Excess of air	Fuel temperature at anode inlet	Post burner exhaust temperature	Air temperature at compressor outlet	Hot fluid temperature at air pre-heater inlet	Air temperature at cathode inlet	Stack voltage	Air mass at cathode inlet	Temperature at anode outlet	Air temperature at cathode outlet
Faults		s_1	s_2	s_3	s_4	s_5	s_6	s_7	s_8	s_9	s_{10}	s_{11}	s_{12}	s_{13}	s_{14}
Air blower fault	f_1	0	1	1	0	0	0	0	1	0	0	0	0	0	0
Air leakage between air compressor and pre-heater	f_2	0	1	1	0	0	0	0	0	0	0	0	0	0	0
Temperature controller failure	f_3	0	1	1	0	1	0	0	0	0	0	0	1	0	0
Pre-reformer fault	f_4	0	0	0	0	0	1	0	0	0	0	0	0	0	0
Stack fault	f_5	1	1	1	0	1	1	1	0	0	1	1	1	0	0

Figure Captions

Figure 1 – Model-based fault detection scheme: X and Y are the control and the measured variables, respectively, N is the noise and $\hat{Y}$ are the simulated variables.

Figure 2 – SOFC system scheme, adapted from [1] and [4].

Figure 3 – Fault Tree for the SOFC air blower [4].

Figure 4 – Example of a symptom type behaviour at different threshold levels.

Figure 5 – Threshold setting process according to false alarm and missed fault probability, adapted from [37]; comparison between deterministic (upper) and probabilistic (lower) residual evaluation process.

Figure 6 – Integration of physical knowledge-based and model-based approaches for FSM robust development.

Figure 7 – Increase in the blower power (a) and outlet temperature (b) due to the mechanical efficiency reduction of about 10%, with respect to OC1.

Figure 8 – Variation of the pre-reformer temperature (a) and hydrogen molar flow (b) due to the heat exchange surface reduction, with respect to OC1.

Figure 9 – Faults simulation results: comparison among the residuals and the defined thresholds at 1% (red straight-dot line) and at 5% (green dashed line) of the monitored variables values at normal conditions; all the considered faults but f_3 have been simulated with respect to OC1, whereas the fault f_3 residuals have been evaluated with respect to OC2.

Figure 10 – Faults simulation results for operating condition influence analysis; all the considered faults but f_3 have been simulated with respect to OC2, whereas the fault f_3 residuals have been evaluated with respect to OC1.

Figure 11 – Fault simulation result for fault f_4 with a fault magnitude of 10%; the residuals have been evaluated with respect to OC1.

Figure 12 – Faults simulation results for fault magnitude influence analysis: the fault magnitude here considered has been set to 50%; all the considered faults but f_3 have been simulated with respect to OC1, whereas the fault f_3 residuals have been evaluated with respect to OC2.

Figure A.1 – Schematic representation of the pipe connecting the air blower and the air pre-heater.

Figure A.2 – Schematic representation of the air leakage into the pipe from a hole of diameter D_H.

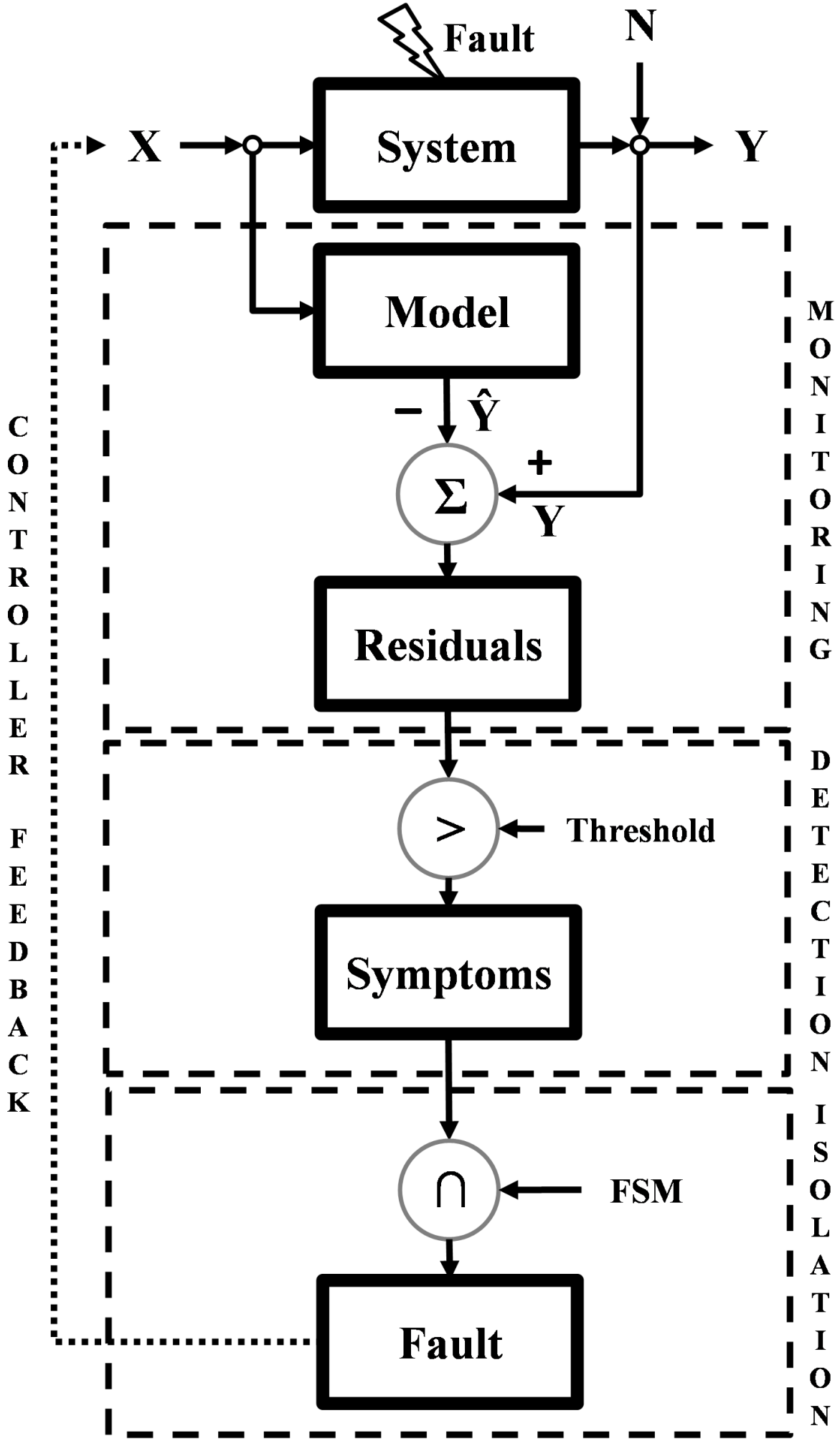
Fault
N
X
System
Y
Model
MONITORING
CONTROLLER FEEDBACK
−
Ŷ
+
Σ
Y
Residuals
DETECTION
>
Threshold
Symptoms
ISOLATION
∩
FSM
Fault

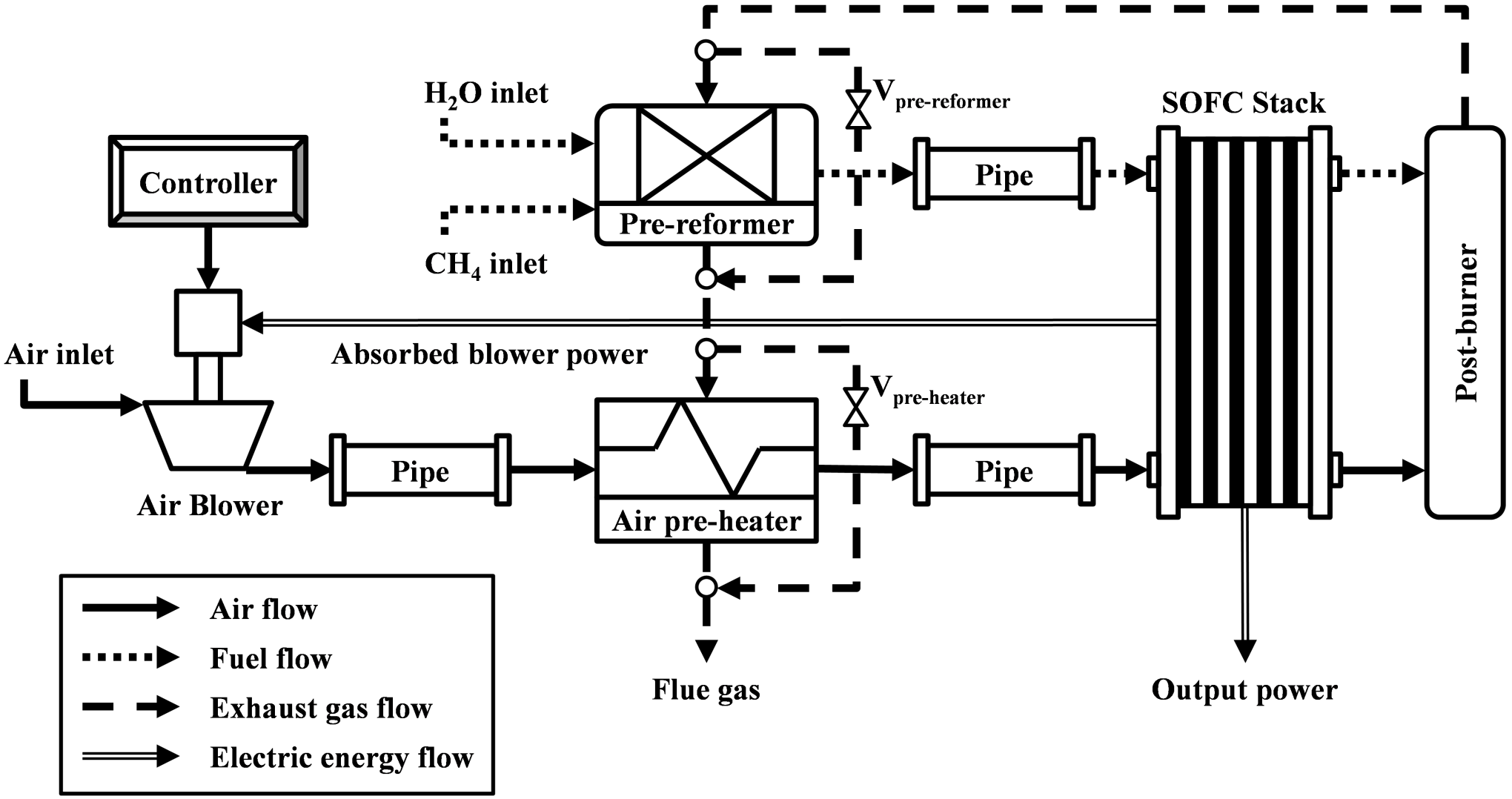

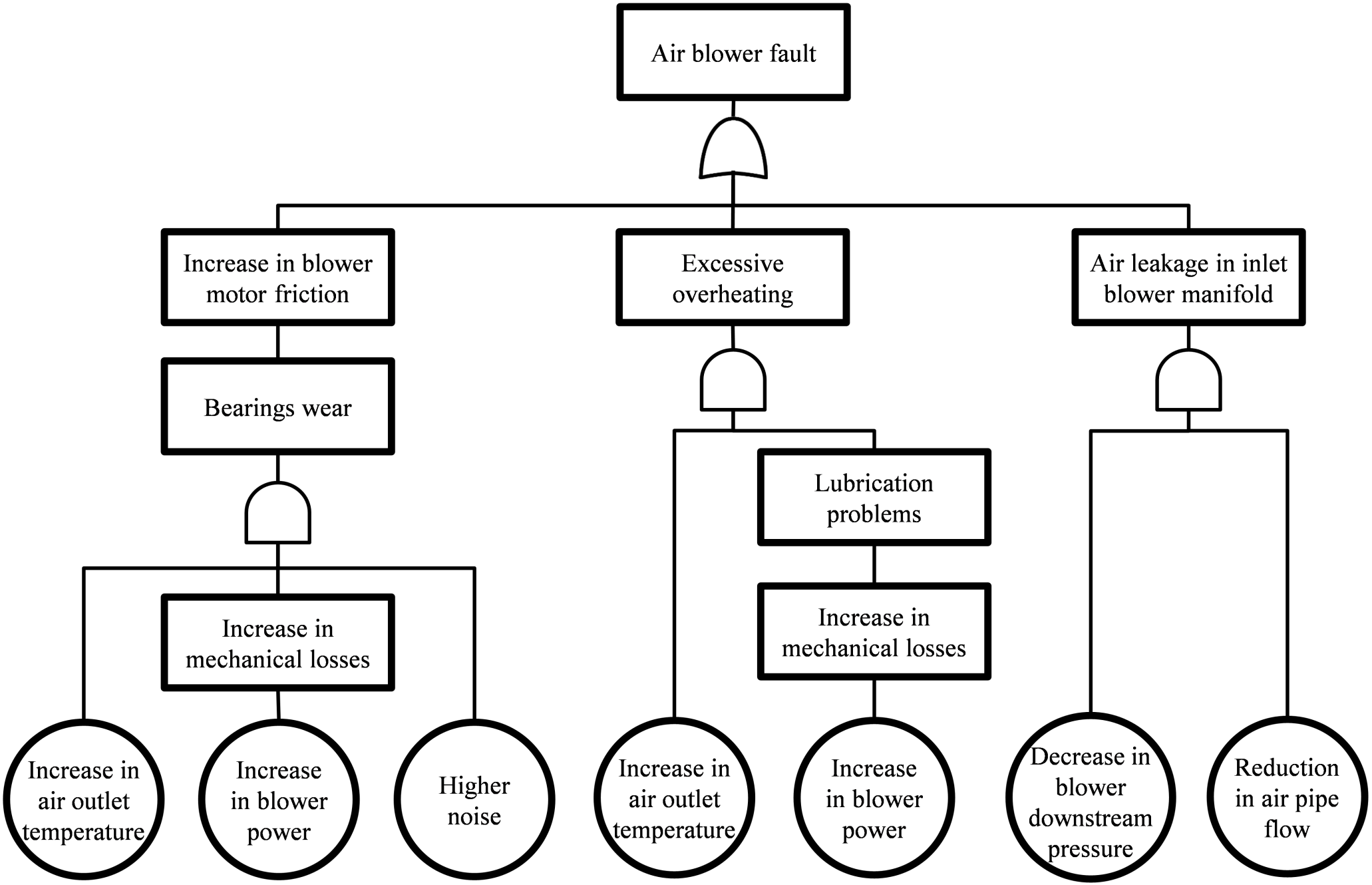

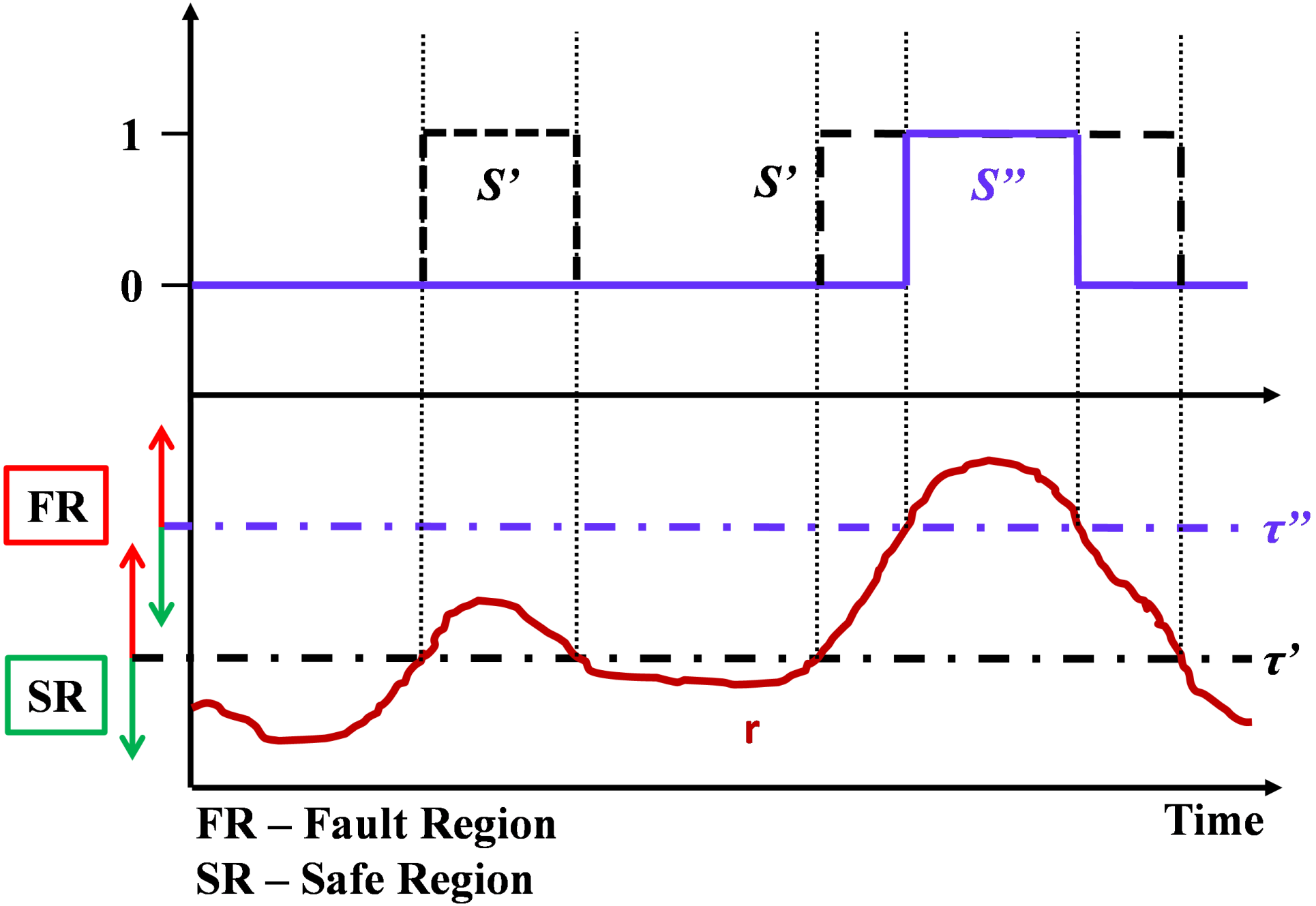

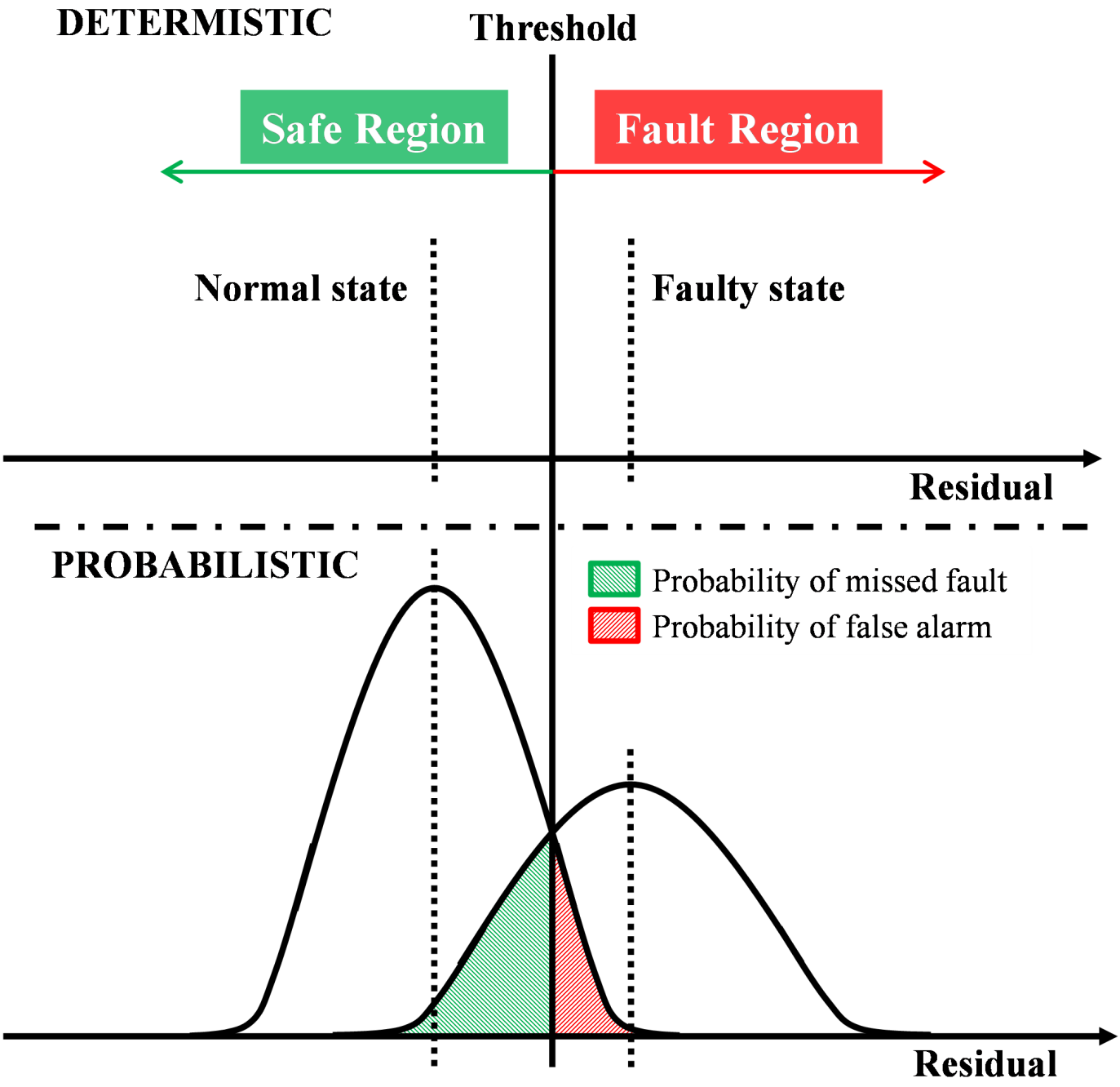
DETERMISTIC
Threshold
Safe Region
Fault Region
Normal state
Faulty state
Residual
PROBABILISTIC
Probability of missed fault
Probability of false alarm
Residual

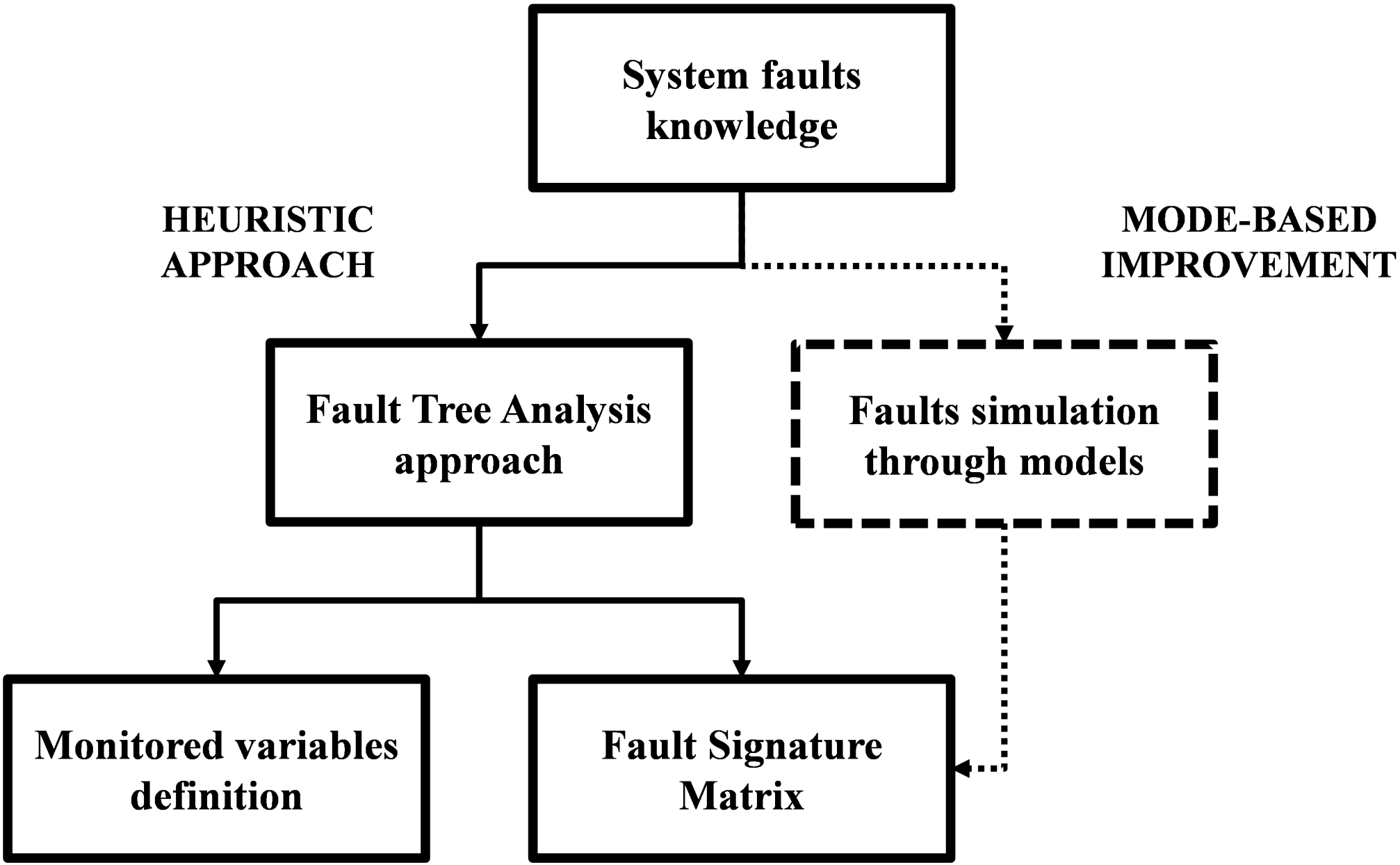

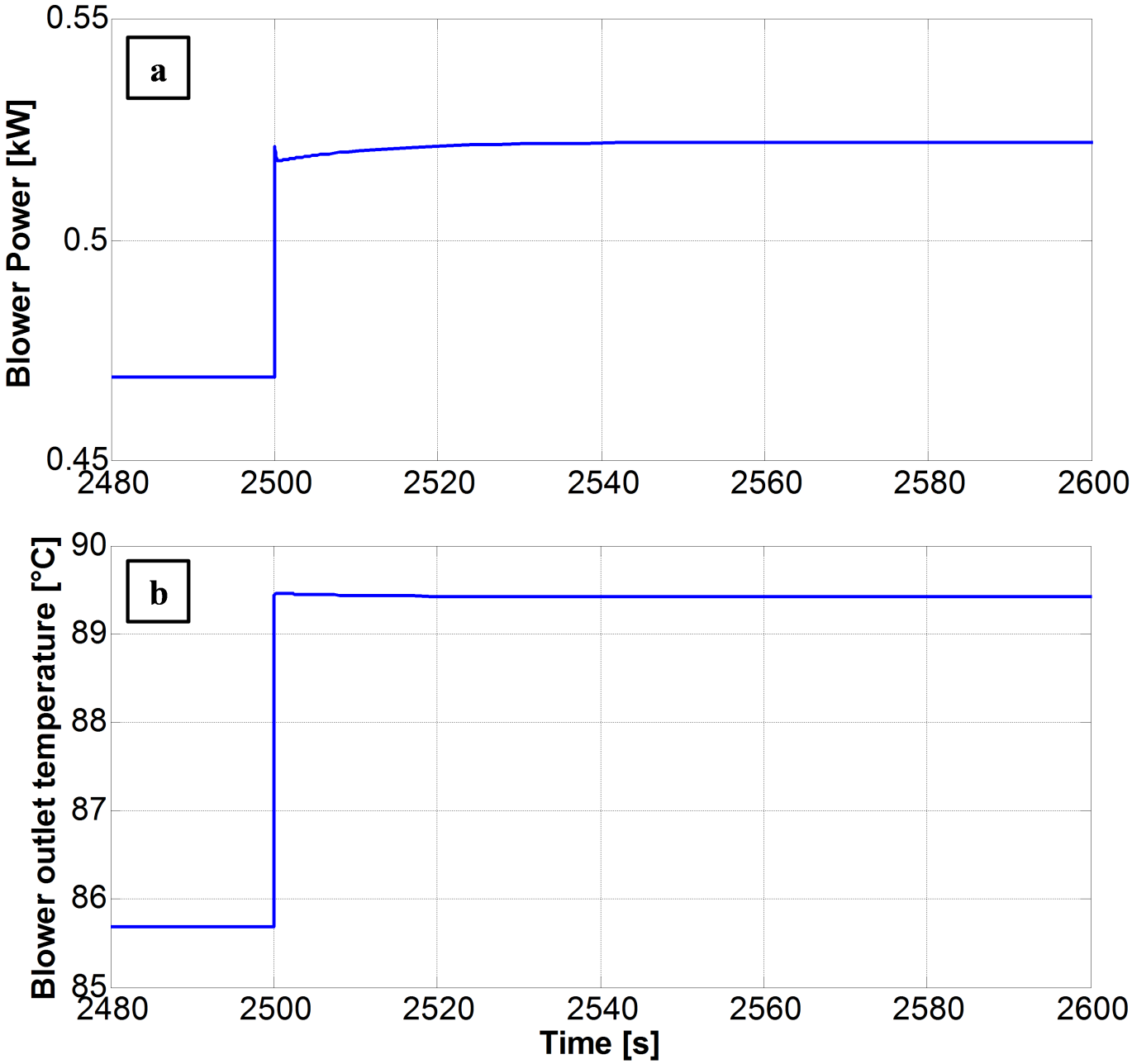
a
Blower Power [kW]
0.55
0.5
0.45
2480
2500
2520
2540
2560
2580
2600
b
Blower outlet temperature [°C]
90
89
88
87
86
85
2480
2500
2520
2540
2560
2580
2600
Time [s]